



1 Modification and validation of a commercial dynamic chamber for reactive

- 2 nitrogen and greenhouse gas flux measurements
- 3 Moxy Shah¹, Kifle Z. Aregahegn¹, Danial Nodeh-Farahani¹, Leigh R. Crilley^{1,‡}, Tasnia Hasan¹,
- 4 Yashar Ebrahimi-Iranpour¹, Fahim Sarker¹, Nick Nickerson², Chance Creelman², Sarah Ellis²,
- 5 Alexander Moravek^{1,§}, Trevor C. VandenBoer^{1,*}

6

- 7 Department of Chemistry, York University, Toronto, Ontario, Canada
- 8 ² Eosense Inc., Dartmouth, Nova Scotia, Canada
- 9 *Now at: Atmospheric Services, WSP Australia, Brisbane, QLD, Australia
- 10 § Now at: German Environment Agency, Department of Air Quality, Dessau-Rosslau, Germany

11 12

*Communicating author: tvandenb@yorku.ca

13 14 15

Abstract

- 16 Reactive nitrogen compounds (NO, NO₂, HONO, NH₃ and others; N_r) play important roles in
- 17 atmospheric processes, and their cascading impacts throughout the Earth system have adverse
- 18 effects on both the environment and human health. The fluxes of these gases at the surface-
- 19 atmosphere interface have been studied in isolation or in smaller subsets by micrometeorological
- 20 techniques or chambers, but simultaneous observations of all N_r species alongside standard
- 21 greenhouse gases (GHGs) as a function of time have not been reported. Here, a dual-dynamic
- 22 chamber system was developed for N_r by modifying a commercially available system for GHG
- 23 fluxes for use with destructive analyzers and to account for chemical changes. The resulting
- 24 platform makes the measurement of N_r and, by extension other reactive gases, more widely
- accessible to the scientific community, as custom chambers do not need to be fabricated.

26

- 27 System modifications to passivate surfaces were implemented, so that N_r gases like NO₂ could be
- 28 effectively transferred to standard gas analyzers, with an initial 36% loss due to transformations
- 29 ultimately minimized below analyzer detection limits (~10%) under relevant atmospheric
- 30 conditions. The modified 72 L chamber did not see a change in the baseline response times for
- 31 GHGs or NO at a flow rate of 2 L min⁻¹. They retained the same values as an ideal non-reactive





trace gas ($\tau = 37\text{-}39$ min versus 36 min. The modifications improved the transfer time constants of NO₂, HONO, and NH₃ by up to 2 min, but substantial surface interactions for NH₃ remain. In all cases, a surface interaction term needs to be characterized for these gases to obtain accurate fluxes. Losses of NO₂ and O₃ by known gas phase reactions, or from deposition and reaction on pristine and aged chamber surfaces, were characterized across a range of environmentally relevant relative humidities (RH) and mixing ratios. The final dual-chamber system configuration includes a measurement and reference chamber, which are necessary to implement the corrections for surface effects and chemical transformations when accurately quantifying dynamic fluxes via a mass balance framework.

Proof-of-concept measurements of N_r fluxes from agricultural soil samples under controlled lab conditions as a function of soil water content were able to quantify emissions of NO, NO₂, HONO, NH₃, and N₂O simultaneously, when subject to fertilization experiments using urea, ammonium carbonate and bicarbonate, and ammonium nitrate. Unfertilized replicate agricultural soil samples showed variability in NO₂ and HONO emissions when prepared with minimal disturbance to the soil structure, with values consistent with those reported by in-situ field measurements. These oppose maximum potential fluxes characterized in prior lab soil manipulations, particularly for HONO relative to NO. Last, fluxes were quantified with destructive gas analyzers in the field with the dual-chamber system on an in-use agricultural soil and included a urea-based fertilizer perturbation to stimulate microbial and chemical transformation and transfer N_r to the atmosphere. The resulting fluxes observed show good agreement with prior reports based on other flux techniques. The mass balance terms within the dual-chamber approach are fully inspected from the pilot deployment in the field, along with an error analysis, to aid in the uptake of this approach by the community.

1 Introduction

- 58 The nitrogen (N) cycle is a crucial biogeochemical cycle on Earth, essential for sustaining life
- 59 through the production of nucleic acids, proteins, and other vital biomolecules (Lehnert et al.,
- 60 2021). Although the carbon cycle receives the most attention due to looming climatic crises caused



79

80

81

82

83

84

85

86

87

88

89



61 by greenhouse gases (GHGs) like carbon dioxide (CO₂) and methane (CH₄), the N cycle is closely 62 intertwined with the carbon cycle (Schlesinger, 2020). At the interface of these cycles and the Earth's surface, reactive nitrogen (N_r) species exchanged between ecosystems and the atmosphere 63 64 have become an area of emerging interest (Lehnert et al., 2021; Wu et al., 2020). Within the atmosphere, N_r species such as nitric oxide (NO) and nitrogen dioxide (NO₂) – collectively referred 65 to as NO_x - ammonia (NH₃), and nitrous acid (HONO) can each be mediated in part through 66 67 surface-atmosphere exchange, influencing local air or water quality, ecosystem processes, and 68 biodiversity (Lehnert et al., 2021; Richardson et al., 2023; Wu et al., 2020). Meanwhile, the non-69 reactive nitrous oxide (N₂O) has climate impacts due to its long atmospheric lifetime (~120 years) 70 and potent greenhouse effect (IPCC, 2023). 71 Reactive nitrogen compounds (NO, NO₂, HONO, and NH₃; N_r) play an important role in 72 atmospheric processes, contributing to the formation of pollutants like ozone (O₃) and secondary 73 organic aerosols (SOA). The exchange of N_r between the Earth's surface and the atmosphere 74 involves numerous production and loss processes driven by both natural and human activities. 75 Reactive nitrogen species are removed from the atmosphere through wet and dry deposition, and 76 their abundance depends on the net outcome relative to N_r emissions (Delaria & Cohen, 2023). At the land surface, N_r is released into the atmosphere by microbial nitrogen cycling, agricultural 77

challenge due to its high spatial and temporal variability driven by factors like climate, vegetation cover, and soil/surface properties (Ludwig et al., 2001). For example, recent studies have demonstrated that HONO production at the ground surface plays a major role in the unexplained daytime HONO source and its impact on daytime OH, with vertically resolved measurements confirming that the surface remains a dominant source at all times of day (VandenBoer et al., 2013, 2015; Young et al., 2012). Such observations pose a challenge in studying N_r because suitable equipment for high time resolution atmospheric observations is expensive, limiting the concurrent study of the interplay between emission and deposition for many N_r species to one or

activities, wildfires, or fossil fuel combustion (Benedict et al., 2017; Mosier, 2008; Yang et al.,

2024). Despite the wealth of knowledge on the environmental importance of N_r , studying N_r at the

surface-atmosphere interface with high time resolution and chemical speciation remains a

a few species at a time. As a result, no systems are currently accessible enough to the scientific





community that they may be deployed across widely different global landscapes, but particularly 91 soils. 92 Soils play a pivotal role in mediating N_r emissions due to their dual function as both a source and 93 a sink of nitrogenous species. Soil-atmosphere exchange of N_r is thought to be governed by 94 microbial processes such as nitrification and denitrification, with soil factors like pH, moisture, 95 organic matter, and nitrogen availability playing a crucial role in regulating N_r emission (Mosier, 2008; Purchase et al., 2023; Stepniewski et al., 2015). These microbial processes have been 96 97 demonstrated to drive the formation and release of some N_r species (e.g., NO, NH₃ and N₂O) in 98 addition to assertions that they can support the production and release of HONO via partitioning 99 (Butterbach-Bahl & Dannenmann, 2011; Kool et al., 2010; Mushinski et al., 2019; Oswald et al., 100 2013; Su et al., 2011). Understanding the exchange of these gases is essential for unravelling the 101 complex interactions between the nitrogen and carbon cycles and their broader environmental 102 impacts from an unprecedented imbalance in the global nitrogen cycle (Richardson et al., 2023). 103 Given the importance of N_r in atmospheric chemistry and its influence on ecosystem processes, it 104 is essential to understand the mechanisms driving its exchange (Fowler et al., 2013). To date,

comprehensive exchange systems for studying the full suite of N_r have not been reported.

106 107

108

109

110

111 112

113

114

115

116

117

118

119

120

105

To quantify N_r exchange for a few explicit species near the ground surface, various flux measurement techniques have been employed, yielding insights into their magnitude and identifying some driving factors. Quantifying fluxes of atmospheric gases has been most effectively applied to GHGs at the surface-atmosphere interface. Traditional measurement methods, such as eddy covariance (EC), relaxed eddy accumulation (REA), and aerodynamic gradient (AG) methods, have been extensively used for ecosystem-scale, continuous flux monitoring, including targeted assessment of most N_r species (e.g., (Bao et al., 2022; Geddes & Murphy, 2014; Kamp et al., 2020; Laufs et al., 2017; Min et al., 2014; Moravek et al., 2014, 2019; Ren et al., 2011; Von Der Heyden et al., 2022; Wang et al., 2022; Wolff et al., 2010). These micrometeorological techniques measure concentrations, concentration gradients, and/or turbulence to estimate fluxes across interfaces applicable to ecosystem-scale processes. When operated continuously, they offer long-term insight without disrupting the natural system. Chamber methods have some advantages compared to micrometeorological techniques, as they are relatively inexpensive, easy to deploy, and require minimal prior meteorological training and





135

136

137138

145

146

147148

Ianniello, 2014).

122 study the effect of different fertilizer treatments (Tang et al., 2020). The chamber method is a widely used technique for measuring GHG fluxes, especially for N₂O. However, challenges remain 123 in addressing potential biases introduced by chemical transformations occurring within the 124 125 chamber and interactions with the chamber surfaces, particularly for N_I species (i.e., NO₂, HONO, NH_3). 126 127 Chemical transformations can occur on chamber surfaces or between the point of emission and 128 measurement. Surface interactions such as adsorption, desorption, and heterogeneous reactions 129 can alter the apparent concentration of several N_r species. For example, NO in a chamber could 130 react in the gas phase with O₃ to form NO₂ during the day and NO₃ at night if sufficient O₃ is 131 present to fully titrate NO (R1, R2). Heterogeneous reaction of gas-phase NO₂ on surfaces under 132 humid conditions also produces nitric acid (HNO₃) and HONO (R3) (Kleffmann et al., 2005; 133 Ramazan et al., 2004; VandenBoer et al., 2015). The formed HONO can undergo multiphase processes in the chamber or on enclosed surfaces by partitioning into water according to its 134

Henry's Law constant and then dissociating into nitrite (NO₂) and the hydronium ion (H₃O⁺)

according to its acid dissociation equilibrium constant and the pH (R4, R5) (He et al., 2006; Ren et al., 2020). Nitrous acid could also photolyze, yielding NO and an OH radical (R6) (Spataro &

expertise (Tang et al., 2020). Chambers are limited to small plots, e.g. making them suitable to

 $139 NO + O_3 \rightarrow NO_2 + O_2 (R1)$

140
$$NO_2 + O_3 \rightarrow NO_3 + O_2$$
 (R2)

141
$$2NO_{2(g)} + H_{2}O_{(ads)} \rightarrow HONO_{(g)} + HNO_{3(ads)}$$
 (R3)

142
$$HONO_{(g)} \leftrightarrow HONO_{(aq)}$$
 (R4)

143
$$\text{HONO}_{(aq)} + \text{H}_2\text{O}_{(l)} \rightleftharpoons \text{NO}_2^-_{(aq)} + \text{H}_3\text{O}^+_{(aq)}$$
 (R5)

144
$$\text{HONO} + hv \rightarrow \text{NO} + \text{OH}$$
 (R6)

These processes in/on the chamber can introduce uncertainty in flux measurements. Characterizing and accounting for chemistry and surface effects in chamber-based methods are necessary to obtain accurate flux measurements of N_r species with a chamber-based system. While static chamber systems typically determine the flux from the change in concentration after closing the chamber





150 headspace and retrieve the flux from the concentration difference at the chamber inlet and outlet. With minor modifications, these chambers have previously been applied to agricultural soils and 151 152 natural ecosystems, demonstrating their utility for measuring emissions of gases such as N₂O and 153 NO_x (Maggiotto et al., 2000; Pape et al., 2009). Their ability to create standardized and 154 reproducible conditions makes them particularly advantageous for studying the driving 155 mechanisms behind gas exchange, yet their application to the full suite of relevant N_r species for 156 surface-atmosphere exchange remains unestablished. 157 The dynamic chamber method has been reported for measurements of the exchange fluxes of 158 challenging gases like biogenic volatile organic compounds (BVOCs, such as monoterpenes and isoprene) from vegetation and farmland (Kolari et al., 2012; Mochizuki et al., 2018), 159 160 NH₃ volatilization from cattle manure (Becciolini et al., 2024), N₂O and NO_x from turfgrass 161 (Maggiotto et al., 2000), and NO_x fluxes from grasslands (Pape et al., 2009; Plake, Sörgel, et al., 2015). Scharko et al. (2015) used sealed chambers and Tang et al. (2019), using dynamic chambers, 162 163 were amongst the first to highlight the potential for both HONO and NO_x fluxes from agricultural 164 soils as hotspots impacting atmospheric chemistry, which has been implemented in atmospheric 165 models (Ha et al., 2023; Tian et al., 2024). 166 The complexity of nitrite (NO₂) chemical and biological production and loss in soils, coupled with 167 soil properties facilitating gas exchange of HONO, has led to intense interest and debate around 168 discerning the fundamental controls on its surface-atmosphere exchange (R4, R5) (Barney & 169 Finlayson-Pitts, 2000; Huang et al., 2002; Kamboures et al., 2008; Meusel et al., 2018; Mushinski 170 et al., 2019; Purchase et al., 2023; Song et al., 2023; Sörgel et al., 2015; Wang et al., 2021). The same is true for direct emissions of NO₂ from soils, where evidence remains limited (Huber et al., 171 172 2024; Zörner et al., 2016). Only a handful of field studies have directly measured soil NO2 173 measurements, making it challenging to infer how much NO₂ might be emitted from soils. .Gong et al. (2025) estimates that fertilizer-induced soil NO_x emissions contribute 0.84-2.2 Tg N yr⁻¹ 174 globally, with uncertainties partly due to the lack of NO₂ measurements. Their modelling indicates 175 176 that this underrepresentation likely leads to underestimation of summertime ozone enhancements 177 (0.3–3.3 ppbv) in agricultural hotspot regions. This N_r exchange is intricately linked to agricultural 178 practices, as excessive nitrogen inputs (e.g., fertilizers) amplify emissions of N_r species, namely

cover, traditional dynamic chamber systems use a controlled flow of ambient air through the





- NO_x, N₂O, HONO, and NH₃ from the impacted soils (Degaspari et al., 2020). These issues highlight the need for more direct soil NO₂ and HONO measurements, as well as simultaneous constraints on the entire N_r suite being exchanged from soils.
 Automated dynamic chambers deployed in situ for field observations would provide a platform for capturing (and manipulating) the magnitude, direction, and temporal variability of N_r species
- or physical variables via the headspace gas or soil amendments while retaining soils in an intact state (Aneja et al., 2006). Thus, establishing an accessible dynamic chamber method for N_r flux measurements is desirable. However, such a platform needs to undergo extensive validation to
- reduce flux bias from challenging N_r species such as NH₃. This important and necessary first step will allow a wider global study of surface-atmosphere N_r exchange processes.
- 189 Here, we modify commercial dynamic chambers originally designed for GHG flux measurements 190 to make them suitable for quantifying the most prevalent N_r gas exchange fluxes at surface-191 atmosphere interfaces. First, we implement surface and hardware modifications to adapt the 192 commercial chambers to minimize gas adsorption and transformations. We systematically 193 characterized the transfer of both GHGs and N_r species by calculating fill and empty rates, 194 transformed to time constants, to identify any surface interactions and/or transformations on the 195 chamber surfaces. We then applied our modified commercial dynamic chambers to make flux 196 measurements by equipping them with destructive gas analyzers for HONO and NO_x and a cavity 197 ring-down spectrometer (Picarro G2509) for NH₃, N₂O, CO₂, and CH₄ in lab experiments, or with 198 a fully automated dual-chamber approach under field conditions through a pilot study. Flux bias 199 minimization through a mass balance approach during the pilot study in a real agricultural field is 200 demonstrated for several N_r gases. This community-accessible approach addresses key needs in 201 allowing more researchers to measure N_r exchange at the surface-atmosphere interface, with the 202 capacity to monitor fluxes of all species simultaneously with at least hourly time resolution.
- 203 **2. Materials and methods**

- 205 **2.1 Dynamic Chambers for Field Fluxes**
- 206 **2.1.1 Description of the custom-modified dual-dynamic chamber system for flux** 207 **measurement**





The dynamic chamber system is composed of two identical commercially available chambers 208 209 (eosAC-LT Eosense, Dartmouth, NS). These are modified and coupled to programmable valves that control the delivery of sample gases to a suite of instrumentation (Figure 1) to perform reactive 210 211 gas flux measurements. 212 The dynamic chambers, constructed out of transparent polyacrylate walls and lids, have an internal volume of 0.072 m³ and can enclose a surface area of 0.21 m². When used on soil surfaces, the 213 chambers are secured with embedded soil collars using custom-made polytetrafluorethylene 214 215 (PTFE) rings (Figure S1) and can be similarly affixed to impervious surfaces. A built-in fan 216 ensures uniform distribution of gases inside the chamber. Ambient air temperature is measured inside the chamber from the fan arm, whereas pressure sensors are embedded in the control box 217 218 outside the chamber. Each chamber has two auxiliary ports, one internally and the other externally, 219 capable of collecting measurements of environmental properties such as relative humidity (RH), 220 photosynthetically active radiation (PAR), soil temperature, and soil volumetric water content 221 (VWC). 222 For a N_r sampling approach, one of the two chambers is used as the measurement (MC) to enclose 223 an experimental surface while the second chamber acts as a reference (RC) by being sealed at the 224 bottom with a film of 0.002" perfluoroalkoxy alkane (PFA; McMasterr-Carr®, PN: 84955K24). 225 The inert PFA film is held in place between the chamber collar and our custom-made PTFE rings 226 (Figure S1). This modification provides a negative control observation for physical interactions on apparatus surfaces and associated chemistry when sampling reactive gases. The use of the RC, 227 therefore, is to facilitate the correction of surface-mediated effects, reactions, and reduction of bias 228 229 when determining quantitative flux values.



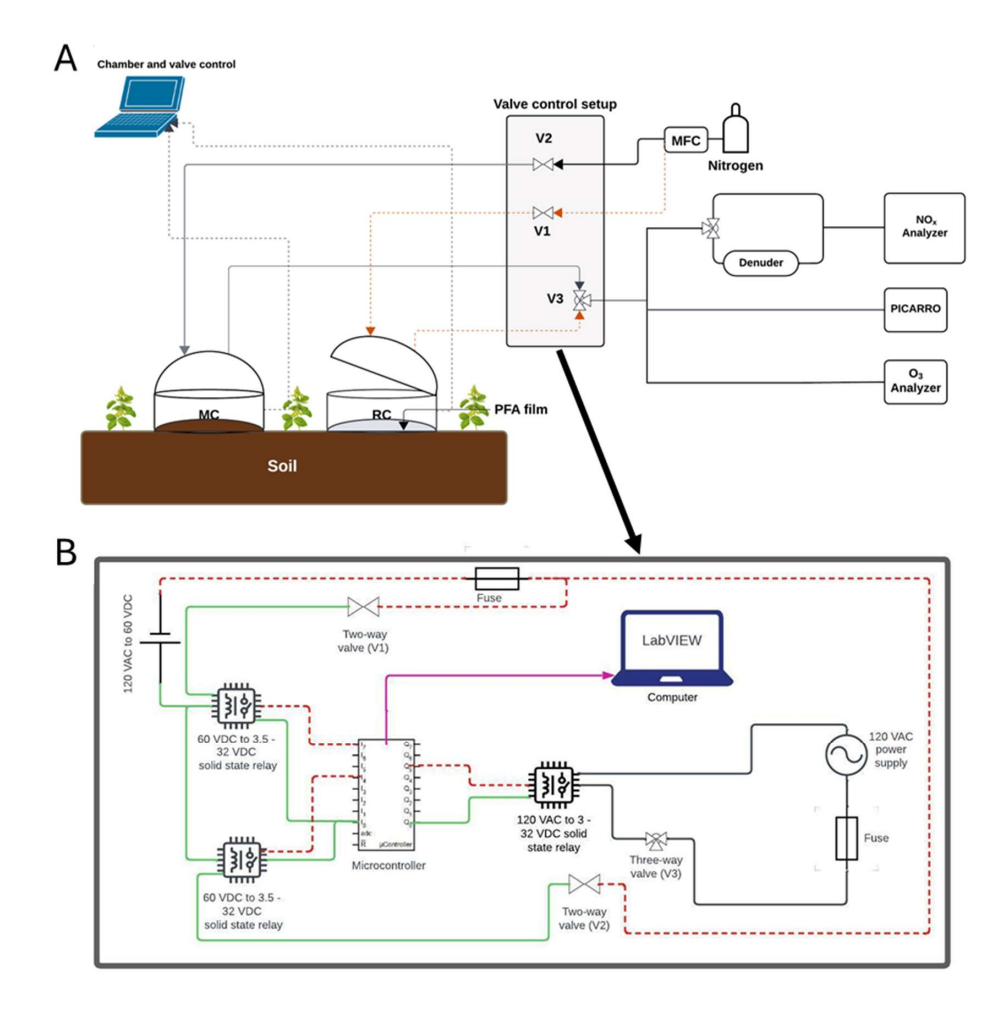


Figure 1. (**A**) Schematic of the dynamic chamber system to measure N_r and GHG fluxes. The components of the system include: the chambers, a dilution gas source (nitrogen (N₂) or zero air (ZA)), solenoid valve control, gas transfer lines, and gas analyzers. Grey lines indicate dilution gas flow from a source (e.g. cylinder) to the measurement chamber (MC) and air sampled from the MC to the analyzers. The dashed orange line represents these same flows relative to the reference chamber (RC). Communication lines from the chambers to a computer for automated control and ancillary sensor data collection using the chamber software (eoslink-AC; blue dotted lines). (**B**) The valve control setup for flow control in the complete dynamic chamber system, illustrating electrical components and lines needed for full automation using LabVIEW. It includes two 24 V DC two-way valves (V1 and V2; red dashed lines for negative electric potential, green for positive), with power supplied by solid-state relays, and a three-way 120 V AC valve (V3; black lines) with a power supply and another solid-state relay. The purple arrow represents the USB data acquisition connection from the microcontroller to a computer running the LabVIEW VI for valve control.





Reactive gases require continuous correction for surface interactions and/or transformations as 245 246 ambient levels are dynamic, so the RC component of this system design continuously baselines 247 the physical interactions and chemistry happening on its surfaces both before and after quantifying 248 reactive gas fluxes with the MC. Thus, the measurements are taken every 30 minutes, where one 249 chamber is closed for gas analysis while the other is open to the ambient atmosphere. The sampling 250 time interval was determined based on the lower limit of the range of field HONO flux values 251 reported in the literature to ensure detection in its application during our pilot field study (see 252 Section 2.6). The resulting accumulated mixing ratios of HONO in the chamber are well above the 253 1.4 parts per billion (ppbv) mixing ratio detection limit (LOD) of even a modified NO_x analyzer, 254 such that it can be used for measuring HONO (Crilley et al., 2023; Lao et al., 2020; Zhou et al., 255 2018; Nodeh-Farahani et al., 2021). 256 Headspace recirculation to facilitate analyte mixing ratio enhancements for non-destructive 257 spectroscopic GHG analysis is a common measurement approach to decrease flux observation 258 times. Reactive nitrogen measurements, in contrast, are typically destructive techniques that 259 change the identity of the target analyte in the act of quantifying its abundance. To interface with 260 such instruments, the sampled air needs to be replaced (Linde Canada Plc, PN: NI LC250-230) to 261 balance the flow demand in a closed chamber. This balance is delicate even when using mass flow 262 controllers (MFCs) on both incoming and outgoing flows, and the best solution we identified is to 263 provide a slight overflow that takes advantage of the chamber design to vent excess pressure 264 through a short length (~15 cm) of 1/8" ID, 1/4" OD tubing that keeps the internal pressure 265 equivalent to ambient. The flow differential between make-up gas and sampling is roughly 400 266 cm³ min⁻¹. Such a supply of make-up gas was explored across a range of potential flow rates when using destructive gas analyzers (e.g., three instruments each sampling at 1 - 4 standard litres per 267 minute, L min⁻¹) to find that 6 L min⁻¹ is the upper limit of flow-through where the chamber 268 269 pressure is not substantially perturbed from ambient and the chamber lid retains its seal. 270 In the field, a flux measurement cycle begins with closing the RC while the MC is open. At defined 271 intervals, they alternate their open-closed states. Flows of make-up gas to each chamber are 272 modulated with a pair of two-way solenoid valves. When sampling from the RC, one valve (V1; 273 Figure 1) is open to permit make-up gas flow while the other valve (V2) is closed to prevent the 274 flow from being directed to the MC. On the sampling lines, a three-way solenoid valve (V3)





275 alternates to guide flow from whichever is closed to the suite of gas analyzers. In this work, the

gas instrumentation included a modified NO_x chemiluminescent analyzer (NO, NO₂, and HONO),

a greenhouse gas and ammonia cavity ringdown spectrometer (H₂O, CO₂, CH₄, N₂O, NH₃), and a

278 UV-absorption ozone (O₃) analyzer. All instrument and operational details are provided in Section

279 2.3.

280

281

282

289

290

291

294

296

297

298

299

2.1.2 Automated controls: system, data collection and processing

The chamber eosLink-AC software (Eosense Inc., Dartmouth, NS) is used to define the duration

of chamber opening and closing cycles, and logs chamber temperature, pressure, and auxiliary

sensor data associated with a given eosAC-LT chamber. Each chamber requires a 12 V DC power

supply connected by USB to a laptop through a weatherproof communication cable, controlling

286 the chamber lid and data transfer.

When a chamber cycle begins, a text file is generated and includes measurement time elapsed,

288 chamber lid status, chamber temperature and pressure, and auxiliary sensor data. This data file is

updated at least once every 10 seconds, varying between 2-8 second intervals, which we average

onto a 1-minute time base to match measurements from the slowest gas analyzers. The solenoid

valves are modulated by the electrical circuit shown in Figure 1B. Automation is facilitated by a

292 microcontroller (NI-6509i, National Instruments) programmed with a custom-scripted LabVIEW

293 VI (LabVIEW version 2020). The VI controls valve states (i.e., for V1, V2, and V3) and

synchronization of the valve switching with respect to each chamber opening and closing cycle as

295 described in the previous section. The VI also generates its own text file containing valve

open/close state and a timestamp to be used for data processing. A custom R script (R Studio

v3.0.1) was developed to process the data file generated by eoslink-AC, data from all reactive gas

analyzers, and the VI. Further design information and full details of this sampling strategy and

script can be found in Section S1 of the supporting information, and is available on the GitHub

repository alongside our VI (https://github.com/fjs-vdblab/fluxchamber.git).

301

302

2.1.3 Reactive and greenhouse gas instrumentation for flux measurements

303 The mixing ratios of NO and NO₂ were measured using a commercially available

304 chemiluminescent NO_x analyzer (EC 9841, American Ecotech, Warren, RI). The calculated LOD





determined from sampling dry zero air was 0.84 ppbv, 0.67 ppbv and 1.07 ppbv for NO, NO_x, and NO₂, respectively. The instrument has an operating range of 0 – 20 parts-per-million by volume (ppmv), a sample flow rate of 0.5 L min⁻¹, and reports measurements at a time resolution of 1 minute. To quantify NO₂, it is reduced to NO on a heated molybdenum catalyst (325 °C). To prevent interferences from atmospherically-relevant acidic species in this system (e.g. HONO, HNO₃, and N₂O₅) the sampled air from the chambers during field experiments was passed through a sodium carbonate (Na₂CO₃) coated annular denuder to reduce bias in the NO₂ measurement, as these species and other components of NO_y (e.g. peroxyacetyl nitrate; PAN) may also be reduced to NO (Villena et al., 2012). The Na₂CO₃ denuder was prepared according to the EPA Compendium Method IO-4.2 (Winberry Jr et al, EPA, 1999) to remove atmospheric acids by reactive uptake to the basic coating. As part of our controlled laboratory and pilot field study experiments, this denuder was also used to selectively measure HONO by scrubbing this target gas for a specified period.

A commercial O_3 analyzer (Serinus 10, American Ecotech, Warren, RI) was used to measure mixing ratios, quantify O_3 loss to surfaces, and constrain the reaction of O_3 with NO to form NO_2 in the pilot study sampling. This analyzer employs a non-dispersive UV absorption cell to quantify O_3 in the sampled air. The calculated LOD from sampling zero air is 0.95 ppbv at 1 minute time resolution, with an operating range of 0 to 20 ppmv and a sampling flow rate of 0.5 L min⁻¹. Quality control procedures for the NO_x and O_3 instruments can be found in Section S2.

The mixing ratios of greenhouse gases (GHGs) and ammonia (NH₃) sampled from the automated chamber system were measured using a Picarro G2509 which uses cavity ring down spectroscopy (CRDS) to simultaneously measure nitrous oxide (N₂O), methane (CH₄), carbon dioxide (CO₂), and NH₃ at ppbv levels, as well as water (H₂O) vapor at ppmv. The analyzer has a time response of ~ 8 seconds for N₂O, CH₄, CO₂, H₂O and < 2 min for NH₃. The Picarro G2509 instrument was used for measurements during both the lab experiments and the pilot study campaign. The customized version of the instrument had a sampling flow rate of ~0.23 L min⁻¹, and was equipped with an inlet filter. To minimize adsorption and chemical interactions of NH₃ on instrument surfaces, stainless steel gas handling components, including the inlet bulkhead, were replaced with PFA counterparts. The instrument cavity material was treated with a SilcoNert® coating by the





manufacturer. The Picarro G2509 analyzer utilizes cavity ringdown spectroscopy to quantify the mixing ratio of the target analytes, and a full span calibration is not necessary to be performed regularly. Despite this, we validated its calibration and performed quality control checks in our laboratory to ensure the accuracy and stability of the analyzer for all aspects of this work presented below (Section S2).

2.2 Chamber modifications to minimize NO₂ reactions on chamber surfaces

To transfer reactive gases through these chambers, interactions with surfaces need to be limited at all points of potential adsorptive or reactive losses. The custom-made base plate, consisting of two rings made from PTFE sheets with a PFA film pinned between them (Figure S1) was used to assess gas interactions on chamber surfaces and acts as the RC for field measurements. From this starting point, commercial components were identified for replacement. First, the gas inlet and outlet push-to-connect fittings in the original chamber configuration have plastic grips, with an internal component made of brass, which is informally known in the atmospheric chemistry community to have strong interactions with nitrogen oxides. These brass fittings were replaced with PTFE Swagelok® bulkhead fittings (PN: T-400-1-4) as shown in Figure S2. Similarly, the polyacrylate wall and lid surfaces of the chambers were considered, which are, by design, actinically transparent to ensure PAR is transferred to any contained plants or surfaces. To retain this visible radiation transparency, while also making the surface more inert, we applied 0.002" thin PFA film to the inner surfaces using double-sided tape (Figure S2).

2.3 Chamber modification validation using greenhouse and reactive gases

The design of the chambers by the manufacturer is to transfer GHGs to non-destructive gas analyzers by recirculating the headspace. Before and after our modifications, we had to ensure that the non-reactive GHGs were still transferred through the system. In addition, we challenged the transfer of N_r gases by controlled gas delivery. It was expected that N_r gases could undergo interactions and/or chemical transformations on the chamber surfaces and sampling tubing that would differ between the unmodified and modified variants. Determining the time constants of fill (E1, E2) and decay (E3, E4) of these reactive gases in the chamber allowed us to contrast their behaviour against that expected from a modelled theoretical inert trace gas in our system (Figure





- 366 2). Equations used to model mass transfer in our chambers were derived from Pape et al. (2009).
- The resulting accumulation curve was modelled by the theoretical function:

368
$$\mu_{\text{fill}}(t) = 1 - e^{-\left(\frac{t}{\tau_{fill}}\right)} \tag{E1}$$

$$\tau_{fill} = V/Q_{fill} \tag{E2}$$

- Where μ_{fill} represents the normalized mixing ratio of the gas in the chamber at the time t (min)
- after closing of the chamber compared to the maximum mixing ratio within the measurement cycle,
- τ_{fill} is theoretical accumulation timescale for transfer of an ideal inert gas (min), V is the volume
- of the chamber (0.072 m³), and Q_{fill} represents the total experimental flow rate (2 L min⁻¹).
- Similarly, the theoretical decay curve when emptying the chamber can be obtained, where τ_{emp} is
- 375 the theoretical decay timescale for gas transfer (min) and Q_{emp} is again the total experimental flow
- 376 rate (2 L min⁻¹).

377
$$\mu_{emp}(t) = e^{\left(-\frac{t}{\tau_{emp}}\right)}$$
 (E3)

$$\tau_{emp} = \frac{V}{Q_{emp}} \tag{E4}$$

379 **2.3.1** Instrumentation and materials for control experiments

- 380 Control experiments for the transmission of inert and reactive gases were conducted by filling and
- 381 emptying the chambers with known quantities of the target gases at mixing ratios relevant to the
- 382 atmosphere, as well as in quantities that would accumulate during real observations of modest
- 383 fluxes (e.g. from a fertilized farm field). Measurement of NO, NO2 and HONO was performed
- using the modified NO_x analyzer, the GHGs (CO₂, CH₄ and N₂O) and NH₃ with the Picarro G2509,
- and O₃ with the UV-absorption instrument. Details of the generation of gas concentrations can be
- 386 found in Section S3 of the SI.

387

2.3.2 Filling and emptying experiments with Nr, O₃, and GHGs

- 388 The positive control experiments filled the chambers in both modified and unmodified
- 389 configurations, where the time constants were calculated from the measurements to compare
- 390 against a theoretical inert and perfectly transferred gas (i.e. lost by dilution and removal to
- analyzers only). In each filling experiment, the chamber was flushed with pure N₂ from a liquid
- 392 N₂ dewar (Linde Canada, PN: NI LC250-20) until a stable baseline level of each gas mixing ratio



394

395

396

397

398

399

400

401

402

403

404

405

406

407

408

409

410

411

412

413

414

415

416

417

418 419

420

421



or one of the N_r analytes was delivered into the chamber along with N_2 as the dilution flow at a total flow rate of 2 L min⁻¹, and this was then sampled at a total of 1.8 L min⁻¹ by the analyzers (Figure S4). The gases were added to the chamber from their respective calibration sources until the observed concentration (C) reached the known value being delivered (C_0), within error. Since different mixing ratios of the gases were added for these control experiments, the use of normalized concentrations was necessary to facilitate data analysis and visualization. Where surface interactions could be identified (e.g. for NH₃), the role of surfaces versus air exchange has been explored using double exponential fits (see ES-1 and ES-2 in Section S3) (Crilley et al., 2023; Ellis et al., 2010; Moravek et al., 2019). The gases were emptied back to the initial baseline level observed with clean dilution gas before starting the next replicate or a new filling experiment with a different target gas. Time constants for filling and emptying were then determined by fitting the experimental observations in Igor Pro8 (Wavemetrics, Portland, OR, US). Similarly, the Eosense eosMX multiplexer is designed to coordinate chamber flux measurements using eosAC chambers with non-destructive analyzers, such that headspace can be recirculated while the chambers are closed. One of these devices was characterized for the transmission of GHGs and N_r gases, alongside similar modifications. This system is appealing as it has the eosLink-MX software (Eosense, V1.9.07), which is used for communication, scheduling actions, and logging peripheral data from all connected eosAC chambers. It features dedicated chamber tubing inlets and outlets, along with a COMM port supporting up to 12 eosAC chambers. Each chamber channel includes two Swagelok gas fittings for transporting gases to analyzers and for either recirculating, or in the case of N_r measurements, supplying a purging gas to the chamber headspace. To optimize the performance for N_r species, the original stainless-steel (SS) Swagelok fittings and solenoid valves were compared against replacement PFA tube fittings, bulkhead unions (Swagelok, PFA-420-61), and a PTFE 3-way valve (Clippard, NR1-2-12-G2). A 2 L min⁻¹ flow of dry zero air containing the target compounds was passed through either the SS valve with SS fittings or the PTFE valve with PFA fittings for 30 minutes each. The flow was measured before and after the valves to ensure the setup was free of leaks. The ratio of the transferred gas amount

was reached; typically, these were values at the analyzer detection limits. Then, a blend of GHGs





to the nominal was used to identify impacts of surface interactions on quantitative transmission to 423 downstream gas analyzers. Further details are presented in Section S4. 424 2.4. Characterization of NO2 loss on chamber surfaces 425 All losses of NO₂ in the chamber were characterized by the addition of known NO₂ mixing ratios 426 to the chamber under a variety of relevant conditions (Figure S5). The experiments were performed progressively, starting from the unmodified configuration of the chamber, replacement of fittings, 427 and covering the inner surface with PFA film to quantify their efficacy in minimizing NO₂ loss 428 429 and/or transformation on chamber surfaces. 430 Different RH values were produced inside the flux chamber by combining flows of dry zero air 431 (ZA) and one saturated with water vapour by transiting a 500 mL Pyrex impinger filled with deionized water (e.g. equal 1 L min⁻¹ flows combine to an RH of 50%). A high-precision, research-432 433 grade humidity probe (HMP60, Vaisala Oyj, Finland; \pm 3% at 0 - 90% RH, \pm 5% at 90 - 100% 434 RH) was connected to the chamber to confirm the set point by measurement in the chamber. The 435 flow from an NO₂ calibration cylinder (Linde Canada; PN: NI NX5MC-AQ; 5.9 (±5%) ppm) was adjusted using an MFC and combined with a dilution flow of ZA to achieve mixing ratios of 5, 7 436 and 10 ppbv. The total flow rate for these experiments was 2.0 L min⁻¹ and a vacuum pump (62.3 437 438 L min⁻¹, PN: UZ-07061-22, Gast Manufacturing Inc., Benton Harbor, MI, USA) with an MFC (10 L min⁻¹, PN: 1179C01314CR1BV, MKS instruments Inc, Andover, MA, US) was used to make 439 up the sampling flow beyond the 0.5 L min⁻¹ of the NO_x analyzer. The same flow difference stated 440 441 above was maintained in the chamber, using the built-in vent. 442 Quantification of NO₂ and HONO in the air sampled from the chamber can be achieved using the 443 alternating solenoid setup depicted in Figure S5. The sampled air is switched between two channels - one directly to the NO_x analyzer and the other through a Na₂CO₃-coated denuder - modulated 444 every 5 minutes by a three-way solenoid valve (Fluoroware Galtek 1/4" F-NPT 3-way solenoid 445 valve, 115V, PN: 203-3414-415. Entegris Inc., MN, US). When the sampled air flows directly to 446 the analyzer, the total mixing ratio of NO₂ and acidic NO_y species, like HONO and HNO₃, is 447 measured and has been termed NO₂* (Crilley et al., 2023; Lao et al., 2020; Zhou et al., 2019). 448 When the flow is directed through a Na₂CO₃ denuder, it selectively scrubs HONO and HNO₃, 449 leaving behind NO₂ (Possanzini et al., 1983). Under the controlled NO₂ composition used in our 450 experiments, it is expected that HONO will be the only acid present in the sampled air, as such 451





452 experimental systems have been thoroughly characterized by Finlayson-Pitts et al. (2003),, and 453 HNO₃ is retained on the surfaces (R3) (Barney & Finlayson-Pitts, 2000; Huang et al., 2002; 454 Kamboures et al., 2008). As a result, by the differential measurement of mixing ratios recorded in the two channels (E5) every 5 minutes, HONO can be quantified. 455 $HONO = NO_2^* - NO_2$ 456 (E5)457 To quantify the amount of NO₂ lost to the chamber surface relative to the mixing ratio of NO₂ 458 added to the chamber during an experiment, the NO₂ loss fraction (f_{NO2}) is informative for mass balance between the two processes. Comparison of each chamber modification on f_{NO2} helps 459 identify which changes are essential in minimizing losses. Experiments using 5 ppby of NO₂ at 460 461 85% RH added to the chamber were used to quantify f_{NO2} in the unmodified configuration (n=3), to derive an upper limit of irreversible loss to surfaces or chemical loss via surface hydrolysis (R3). 462 Following the materials characterization experiments, additions of atmospherically relevant 5, 7 463 464 and 10 ppbv mixing ratios of NO₂ at three different RH values (45%, 65% and 85%) to the fully 465 modified chamber were used to characterize and develop a correction methodology for the surface 466 loss. The mixing ratios of NO₂ and RH values selected for these experiments are representative of 467 the ambient atmosphere in urban areas (Toronto North Station, ECCC), where the chamber system 468 was envisioned to be deployed. 469 2.5 Drivers of O₃ loss to chamber surfaces 470 We tested how modifications and aging of the interior chamber surfaces affected O₃ transfer. It is 471 among the most sensitive/reactive species to transfer through this new system and is expected to 472 drive reactive loss of NO when measuring N_r fluxes. The fraction of O₃ lost to chamber surfaces 473 was first quantified using a clean and unmodified chamber with PTFE bulkhead fittings replacing 474 the push-to-connect brass fittings. Prior to O₃ addition, the chamber was flushed with ZA until the 475 background level of O₃ was at the instrument detection limits. Three mixing ratios of O₃ of 150, 200 and 250 ppb generated by a GasCal 1100 dilution calibrator with integrated O₃ generator and 476 477 photometer (American Ecotech, Warren, RI) and added to the chamber for 60 mins or until a 478 constant concentration was reached. Two replicate runs of each addition level were performed. 479 The fraction of O₃ lost to chamber surfaces was quantified in duplicate on a modified chamber with the interior chamber surfaces covered by brand new 0.002" thick PFA film in a separate set 480



510



482 operated for lab and field experiments, so that the PFA film had been attached to the inner surface 483 of the chamber and exposed to ambient air for more than two years, with 15 days of continuous 484 use in an agricultural field during our pilot study. In all three experiments, the lost fraction of O₃ 485 was determined for each mixing ratio delivered. 486 2.6 Proof of concept N_r fluxes from agricultural soils 487 2.6.1 Soil sample N_r emissions for lab experiments 488 Randomized soil samples weighing 4-5 kg were collected into Ziplock bags from an eight-plot 489 grid established for an agricultural field site in Lambton County, ON, Canada (43°09'36.0" N 490 81°55'48.0" W). The samples were used to investigate emissions in the lab with and without the 491 addition of fertilizers. Individual and pooled samples from the field plots were used. Bulk soil 492 samples were prepared for lab-based chamber measurements by removing debris, roots and seeds, 493 followed by oven drying at 35 °C for 24-72 hours on a stainless-steel mesh tray covered with 494 aluminum foil, to prevent alteration of the microbial community from exposure to unrealistic 495 temperature regimes. After drying, samples were stored in Ziploc® bags at room temperature until 496 use. 497 Ultrapure water (18 MΩ·cm; Milli-Q®, Sigma-Aldrich, St, Louis, US) was added to approximately 350 g of a dry soil sample to achieve ~28% volumetric water content (VWC). The 498 499 soil sample was loaded into the chamber on a foil-lined tray, and the water content was measured 500 using a soil moisture probe inserted fully into the sample (TEROS 11, VWC range for mineral soils: $0.00 - 0.70 \text{ m}^3/\text{m}^3$; accuracy: $\pm 0.03 \text{ m}^3/\text{m}^3$; resolution: $0.001 \text{ m}^3/\text{m}^3$, METER Group Inc., 501 502 WA, USA). The chamber was then sealed against intrusion from room air, and dry ZA was added 503 to the chamber during the drying period. A modified NO_x analyzer measured NO, NO₂ and HONO 504 following our usual configuration, while the Picarro G2509 measured N2O and NH3 fluxes. Both 505 instruments monitored unamended soil samples and others fertilized with urea (CO(NH₂)₂), 506 ammonium carbonate (AC, (NH₄)₂CO₃), ammonium bicarbonate (ABC, NH₄HCO₃) at rates of 100 kg N ha⁻¹. A similar experiment was conducted with ammonium nitrate (NH₄NO₃) at the same 507 508 fertilizer rate using only the modified NO_x analyzer. Soil VWC and headspace RH were recorded

2.6.2 Field deployment of automated dynamic Nr chambers

using auxiliary sensors within the chamber.





The RC and MC setup was deployed to make automated N_r flux measurements from the same agricultural field as the lab-based soil samples described in the prior section. The observations took place in early September 2022 at the end of a soybean cropping season. A detailed description of the campaign and its results is the subject of a separate work, so we provide a brief overview here relevant to demonstrating the utility and procedure of an RC/MC chamber pair to determine fluxes from field observations. The total measurement period was approximately two weeks in duration to test the performance of the designed system. Generally, conditions were hot and dry, without precipitation, and the soybeans surrounding the observed soils were undergoing senescence during the measurement period. The chambers were deployed only on the soil, between crop rows, and operated to quantify fluxes as outlined in Section S7. After an initial 7-day period of observing baseline fluxes from the field, an experimental perturbation was conducted to stimulate N_r emissions through the addition of an aqueous urea solution equivalent to 22 kg N ha⁻¹ of fertilizer added by broadcast application, followed by washing into the soil by an equivalent of 2.5 cm (1") of rain. The modified NO_x analyzer and the Picarro G2509 were used to measure the N_r and GHG fluxes continuously across both periods.

2.7 Soil flux determination

The flux of a gas is the rate at which it is released and/or transferred across a surface or an interface (e.g., soil to atmosphere) per unit area per unit time. Gas fluxes are of high interest in agriculture as they give insight into the uptake or emission of N-bearing gases that may lead to fertilizing, or loss of fertilizing effects, respectively. Fluxes are also important for assessing the state of plants or soils at interfaces through metrics like primary productivity, in which case measurement of a GHG like CO₂ provides the insight (Anthony & Silver, 2024; Li et al., 2016; Okiti et al., 2025). The RC captures environmental fluctuations such as temperature or pressure change and directly observes the interactions of ambient gases with surfaces within the sampling setup, as well as tracking reactions, allowing for corrections to every net flux (F_{net}) measurement cycle (E6 for reactive gases and E7 for non-reactive gases, as derived in Section S7).

537
$$F_{\text{net}} = (\lambda) \cdot \left(\frac{V}{A} \left(\frac{\Delta C_m}{\Delta t_m} - \frac{\Delta C_r}{\Delta t_r} \right) + \frac{Q_{\text{out}}}{A} \left(\frac{\int_{t_{1m}}^{t_{2m}} c_m(t) \ dt}{\Delta t_m} - \frac{\int_{t_{1r}}^{t_{2r}} c_r(t) \ dt}{\Delta t_r} \right) - \frac{V}{A} \left(\frac{\int_{t_{1m}}^{t_{2m}} R_m(t) \ dt}{\Delta t_m} - \frac{\int_{t_{1r}}^{t_{2r}} R_r(t) \ dt}{\Delta t_r} \right) \right)$$

E6





Where V is the volume of the chamber (m³), A is the surface area (m²) enclosed by the chamber 539 540 and governing the gas flux; Q_{out} is the volumetric flow rate of air exiting the chamber (m³ s⁻¹; $c_m(t)$ and $c_r(t)$ are target gas concentrations within the measurement and reference chamber (mol 541 m⁻³), respectively; $\frac{\Delta C_m}{\Delta t_m}$ and $\frac{\Delta C_r}{\Delta t_r}$ represent their corresponding rates of change (mol m⁻³ s⁻¹); and F_{net} 542 is the resulting net gas flux per unit area (mol m⁻² s⁻¹). The terms R_m and R_r denote the 543 544 instantaneous chemical production or loss rate expressed in units of mol m⁻³ s⁻¹ for consistency. The dimensionless attenuation factor λ is required to correct for interactions of reactive gases with 545 546 chamber surfaces. Such surface interactions, which are particularly strong for gases like NH₃, significantly reduce the measured rate of concentration change within the closed chamber (Figure 547 548 4). Thus, λ is derived as the ratio between a theoretical unattenuated gas and the target gas 549 concentration from controlled deliveries integrated over the chamber closure interval as derived in 550 Section S7. The attenuation correction removes bias from chamber-induced artifacts in flux 551 estimates, so that more accurate soil-atmosphere exchange is reported.

$$F_{\text{net}} = \lambda \cdot \frac{P_{\text{air}}}{R \cdot T} \cdot \left(\frac{V}{A} \left(\frac{\Delta X_m}{\Delta t_m} - \frac{\Delta X_r}{\Delta t_r} \right) + \frac{Q_{\text{out}}}{A} \left(\frac{\int_{t_{1m}}^{t_{2m}} X_m(t) \ dt}{\Delta t_m} - \frac{\int_{t_{1r}}^{t_{2r}} X_r(t) \ dt}{\Delta t_r} \right) \right)$$

553 **E7**

For inert gases in E7, the fluxes can be based on mixing ratios, where X_m and X_r are the gas volumetric mixing ratios (mol X per mol air), P_{air} is the air pressure (Pa), T is the absolute temperature (K), and R is the universal gas constant (J mol⁻¹ K⁻¹). By comparing the RC and MC observations, we isolate the effects of specific environmental conditions on N_r (E6) or GHG (E7) exchange fluxes, while accounting for surface effects and chemical transformations in the former.

3 Results

554

555

556

557

558

559

560

561562

563

564565

566

3.1 Determining time constants of reactive nitrogen and GHGs

The time constants of both filling and emptying the chambers were calculated using concentrations normalized to their initial values, for each N_r gas and GHG. These were used to quantify gas transfer times through the chambers and to confirm performance relative to theory. Where departures were identified, we quantified the extent of surface interactions for the various target analytes so corrections for determining in situ fluxes could be implemented (Table 1, Figure 2).



568

571

572

573

575

576

577

578 579

580

581

582

583

584



3.1.1 Time constants of greenhouse gases (GHGs)

Determination of the GHG time constants allows benchmarking of the chamber performance prior 569 to and after modifications, which then allows us to contrast the behaviour of transferred reactive 570 gases through the chambers. In both the modified and unmodified chambers, the greenhouse gases CO₂, CH₄ and N₂O were anticipated to behave as non-reactive trace gases with little to no physical interactions on chamber surfaces, nor to undergo chemical transformations. The theoretical fill and empty rates for the chambers with a flow rate of 2 L min⁻¹ are 36 min. The average measured time constants of filling with the greenhouse gases CH₄, CO₂, and N₂O in the 574 unmodified chamber were found to be 37 ± 1 min, 37 ± 2 min, and 37 ± 1 min, respectively (Table 1). During the emptying phase, the average time constants for CH₄, CO₂, and N₂O were 37 ± 1 min, 37 ± 1 min, and 38 ± 2 min, respectively. These measurements are not different from theory within the limits of experimental accuracy, demonstrating that GHGs do not deviate from the values modelled for an ideal trace gas (Figure 2). In either experiment, the time constants did not change in the presence of the chamber modifications. Since the GHGs are effectively transferred through both the modified and unmodified configurations of the chamber, the baseline performance of the chambers was not affected by the hardware modifications. Therefore, comparison of these results with the time constants of N_r gases provides a description of their

interaction or transformation processes on the modified chamber surfaces.



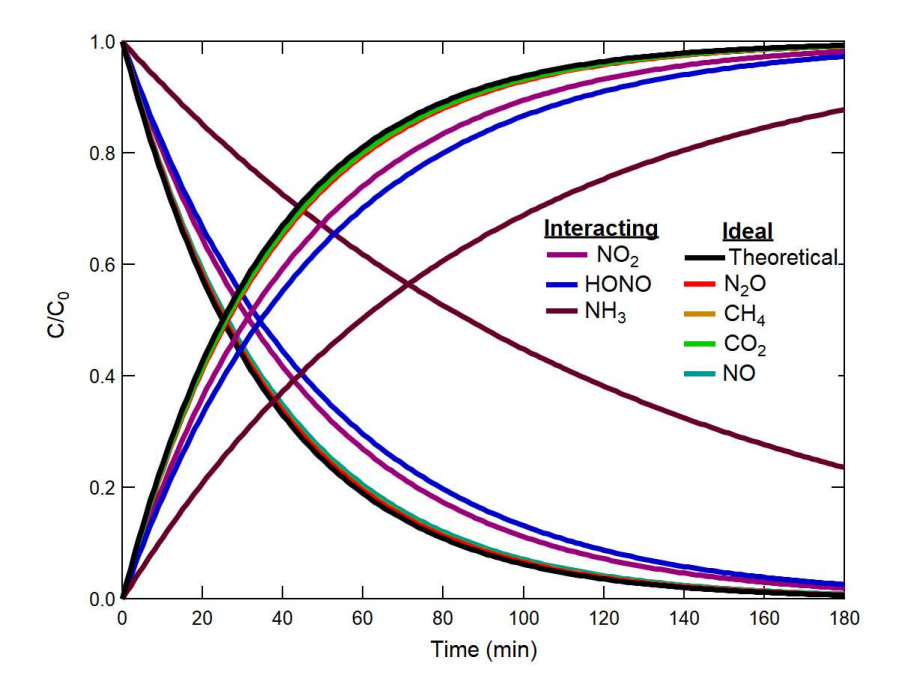


Figure 2. Addition of reactive nitrogen gases and greenhouse gases to a modified dynamic chamber. For clarity, the coloured traces show the fitting curves corresponding to the response time in concentration normalized to the delivered value of each gas while filling and emptying the chamber. The black trace corresponds to a perfect non-reactive transfer of an ideal trace gas based on volume transfer in the chamber only. Note that the N₂O, CH₄, CO₂ and NO fill and empty traces all overlap with the theoretical fill and empty curves.

3.1.2 Time constants of reactive nitrogen gases

In the modified chamber, the time constant of filling or emptying with NO was 38 ± 1 min. The obtained NO time constants are similar to GHGs, as NO is not expected to have strong surface interactions. The slower time response of the NO₂, HONO, and NH₃ measurements is determined by two processes: (1) the exchange of the sample air volume in the inlet line and the chamber, and (2) the adsorption and desorption of the gas onto and from the chamber surface (Whitehead et al., 2008). Increases in surface interactions were observed for increasingly polar gases in the order of NO₂, then HONO, and most for NH₃ (Figure 2). The highest change in the time constants between the modified and unmodified configurations was 2.6 ± 2.5 min, observed for HONO, with smaller improvements observed for NO₂ and NH₃ during the filling process. Improved time constants





603 when emptying reactive nitrogen from the chambers had similar trends (Table 1). 604 Overall, the deviations for these gases to longer time constants than those expected from an inert 605 molecule can be attributed to their polar, ionizable, and/or reactive nature. For example, NO2 is lost more readily than NO, possibly through its known reaction on surfaces to make HONO and 606 607 HNO₃, being lost itself in the process (Finlayson-Pitts et al., 2003). It also has higher water 608 solubility than NO, but lower than for HONO or NH₃. Similarly, a decrease in transmission efficiency for HONO could be explained by its weakly acidic nature (pKa = 3.16) (Silva et al., 609 610 2006) and solubility in water (Henry's law constant = 0.48 mol/m³ Pa; (Schwartz & White, 1981) 611 that facilitate partitioning and dissociation in surface water films, which could generate non-612 volatile nitrite (NO₂-) on chamber surfaces. This chemistry will slow the transfer of gas-phase HONO through the chambers, as the NO₂ would need to protonate before being lost as neutral 613 614 HONO when repartitioning to the gas phase (R4, R5). Finally, the most delayed transmission rate is for NH3, likely because it undergoes strong inter-molecule interactions and ionization on the 615 chamber surfaces and/or any interfacial water (Henry's law constant = 5.9×10^{-1} mol/m³ Pa (Orkin 616 et al., 2011); pKa = 9.25 (Lide, 2009), as well as on tubing surfaces and potentially partitioning 617 618 into the tubing before reaching the analyzer (Pagonis et al., 2017). 619 The determined surface impact values (D; Table 1) demonstrate an expected greater impact of 620 surfaces when no reactive gas is present in the headspace prior to filling, and a lesser effect during 621 emptying when the surface has been exposed and equilibrated with the analyte, which is commonly 622 referred to as passivation. As a result, increasing delays from NO through NH₃ exist in our N_r gas 623 suite due to increasingly stronger interactions with chamber surfaces and gas handling lines. For 624 NH₃ specifically, the fill has a D value of 89%, while during emptying it is only 23%. This is due 625 to all sample handling surfaces not being passivated prior to filling, similar to our findings with 626 NH₃ transfer for other N_r instruments (Crilley et al., 2023). In contrast, during the emptying process, desorption occurs over previously exposed surfaces ending at the instrument, reducing 627 628 the extent of surface effects. The surface interactions for these gases are minimized in the modified 629 chambers to facilitate more time-efficient measurements of surface exchange. However, they 630 necessitate the use of the λ term when deployed in the measurement-reference configuration for 631 those N_r species which experience partial transmission, such as NH₃. The λ term is required to 632 obtain accurate values, as the enclosed flux measurement surface should be perturbed for the least





amount of time possible when making field measurements, and the chambers cannot be closed for several hours to allow surface-active gases to passivate the lines. In addition, minimizing the potential for transformations reduces the frequency required for in-field characterization of these processes through positive and negative gas delivery controls. For NO₂, specifically, we sought to quantify this as a function of modifying components of our chambers, as NO₂ is the most reactive gas in our suite.

Table 1. Summary of time responses of addition and removal of GHGs and N_r gases to and from a chamber at 2 L min⁻¹ in unmodified and modified configurations. Time responses here correspond to a theoretical fill or empty e-folding time response of 36 minutes. Where analytes were observed to undergo surface interactions, a double exponential fit was used to characterize them, with the first time constant representing the known gas exchange rate being fixed at 36 minutes, as this was observed for the non-reactive gases, and the second time constant is reported (*) alongside an assessment of the relative magnitude of surface interactions, through the D-value (%) (Crilley et al., 2023; Ellis et al., 2010; Moravek et al., 2019). Variability shown is one standard deviation of the mean from replicate experiments (n=3).

Gas species	Direction	Unmodified (min)	Modified (min)	Improvement (min)	D (%)
NO	Fill	38.8 ± 0.7	37.8 ± 0.6	1.0 ± 0.7	-
NO	Empty	37.9 ± 1.5	36.0 ± 0.6	1.9 ± 2.1	-
NO	Fill*	18.9 ± 0.6	18.0 ± 3.1	0.9 ± 3.2	94 ± 18
NO_2	Empty*	21.2 ± 1.2	20.4 ± 1.4	0.8 ± 1.9	78 ± 21
HONO	Fill*	21.9 ± 1.1	19.3 ± 1.2	2.6 ± 1.6	74 ± 10
HONO	Empty*	23.2 ± 1.4	21.2 ± 0.9	2.0 ± 1.7	71 ± 9
NIII	Fill*	69.6 ± 0.4	68.2 ± 0.5	1.4 ± 0.6	89 ± 3
NH ₃	Empty*	76.9 ± 0.8	75.0 ± 4.6	1.9 ± 4.7	23 ± 4
GO.	Fill	37.9 ± 1.5	37.0 ± 1.8	0.9 ± 2.3	-
CO_2	Empty	38.0 ± 1.8	37.0 ± 1.2	1.0 ± 2.2	-
CH	Fill	37.9 ± 1.1	36.8± 1.2	1.1 ± 1.6	-
CH ₄	Empty	$39.1{\pm}~1.7$	37.2 ± 1.2	1.9 ± 2.1	-
NO	Fill	38.6 ± 2.1	36.7 ± 1.2	1.9 ± 2.4	-
N_2O	Empty	39.7 ± 1.3	37.7 ± 1.6	2.0 ± 2.1	-



649

650

651

652

653

654

655

656657

658659

660

661662

663664

665

666

667

668669

670

671

672

673

674675



3.2 Multiplexer modification impacts on gas transfer

The multiplexer (eosMX; Eosense Inc.) allows us to operate up to twelve dynamic chambers simultaneously with a suite of gas analyzers such as the Picarro G2509, NO_x, and O₃ analyzers. However, the commercial multiplexer is constructed with stainless steel (SS) valves and fittings that would be expected to facilitate strong interactions or losses of target gases in the N_r analyte suite. Valves and fittings made of SS have a higher tendency to chemically interact and/or adsorb reactive gases compared to fluoropolymer replacements. To address this uncertainty, the gas transfer efficiency as a percentage loss in the multiplexer versus a bypass line was evaluated specifically for NH₃ and NO₂, alongside standard GHGs as they passed through fittings and gas handling solenoid valves made of SS or PFA and PTFE replacement parts.

The loss fractions were modest and measurable when connected to the analyzers using minimal lengths of PFA tubing (~50 cm). The most substantial loss of gases was observed on SS, in which the highest reactivity and/or adsorption were expected due to its known tendency to interact with reactive gases (Vaittinen et al., 2014). When the GHGs were delivered after dry zero air into the SS setup for 30 minutes, typical of a chamber closure period, their losses ranged from 10% for N₂O to 19% for H₂O. Meanwhile, NO₂ exhibited 17% loss on the SS surfaces, and the greatest effect was seen for NH₃ with a loss of 38% (Figure S6). In contrast, losses on the chemically inert and hydrophobic surface of the PFA fittings and PTFE valve were negligible (<1%) for most gases, except for NH₃, which still exhibited a measurable loss of 11%. Other reports have also shown up to 15% loss of NH₃ at atmospheric pressure on PTFE and PFA surfaces (Ellis et al., 2010; Shah et al., 2006; Vaittinen et al., 2014). While it is expected that the SS would eventually passivate and improve the transmission of the GHGs in a standard recirculation approach, this is not likely to be the case for destructively analyzed N_r and even more so if it facilitates a chemical transformation. Overall, we found that replacing the multiplexer SS valves and fittings with PFA fittings and PTFE valves provided a 9–27% reduction in surface losses of N_r compounds and GHGs. We strongly recommend the use of PTFE and/or PFA materials over SS for more accurate measurement of N_r species when interfacing the dual chamber setup with the destructive N_r analyzers needed for field flux measurements, whether using a custom setup of the commercially available multiplexer.

676

677





689

3.3 Minimizing NO₂ losses and determining controlling variables

679 In addition to the rate of transfer of N_r gases, chamber modifications are necessary to prevent 680 reactive losses. The lost fraction of NO₂ (f_{NO2}) to chamber surfaces was quantified by the addition 681 of known mixing ratios of calibration gas to the chamber in both the unmodified and modified 682 configurations under atmospherically relevant humidities. These experiments enabled us to 683 determine the magnitude of NO2 lost to the chamber and gas transfer tubing surfaces due to 684 chemical and/or physical transformations, as well as demonstrate the effectiveness of the different 685 chamber modifications in minimizing these losses. For NO2, a probable chemical transformation pathway is its heterogeneous conversion to HONO (R3), which is favourable under 686 687 atmospherically relevant humidities, and the resulting water-adsorbed surfaces expected to exist 688 throughout the chamber and sampling lines.

3.3.1. Chamber modification impacts on NO₂ losses

- The average fractional loss (f_{NO2}) for an unmodified chamber and one modified with the PFA film
- 691 and PTFE bulkhead fittings was measured under conditions of 83% RH and 5 ppb of NO₂.
- 692 Substantial reduction in NO₂ loss and transformation was observed from the implemented
- modifications. In the original unmodified configuration of the chamber, f_{NO2} was 0.36 ± 0.02
- 694 (Figure S7). When the interior chamber surfaces were covered with a film of PFA, it was reduced
- to 0.22 ± 0.03 , a relative decrease of 18%. This is consistent with the acrylic chamber surfaces and
- fasteners to the chamber frame, facilitating physical and/or chemical loss of NO₂.
- 697 The film of PFA, along with other fluoropolymers, is known to have excellent chemical resistance
- 698 and low reactivity towards a range of chemicals, including NO₂ (Ebnesajjad, 2005; Graham et al.,
- 699 1997). In addition, the superhydrophobic nature of these materials prevents the accumulation of
- 700 water on the surfaces, which is known to facilitate atmospheric surface reactions of NO₂
- 701 (Finlayson-Pitts et al., 2002; Jenkin et al., 1988; Stutz et al., 2002) and create analytical bias in the
- 702 measurement of trace gases like HONO, especially when instrument gas sampling inlets do not
- take this into account (Crilley et al., 2019; Von Der Heyden et al., 2022).
- 704 The replacement of the brass-lined push-to-connect bulkhead fittings with PTFE led to a similar
- decrease in f_{NO2} , which was reduced by 17% to a final value of less than 0.05 ± 0.02 (Figure S7).
- These fitting surfaces act as the largest surface-driven NO₂ loss despite their surface area being





very small compared to that of the entire chamber configuration and with a very small contact time against the gas sample (0.012 s per fitting at a flow rate of 2 L min⁻¹).

709 The loss of NO₂ in the commercially available system is challenging to attribute solely to the 710 heterogeneous hydrolysis reaction. During the characterization experiments, the conditions inside 711 the chamber were matched to those reported by previous lab studies, which have shown that high 712 RH, presence of NO₂, and surface adsorbed water on surfaces favour this loss mechanism (Jenkin et al., 1988; Stutz et al., 2004). The reaction is known to occur on surfaces such as Pyrex (Jenkin 713 714 et al., 1988) and borosilicate glass (Finlayson-Pitts et al., 2002), but no prior studies to date, nor 715 this study, have demonstrated metallic surfaces as facilitating this mechanism. 716 Overall, chamber modifications were effective in minimizing NO₂ losses. The inert PTFE fittings 717 dramatically minimized transformations, while PFA film lining the inner chamber surfaces was 718 also effective, but less so. Our results indicate that water-adsorbed and metallic surfaces, such as 719 brass, facilitate substantial loss and/or transformations of NO2. Further investigation is required to

721

722

723724

725

726727

728

729

730

731

732

733

734

735

720

3.3.2. RH-facilitated NO₂ loss as a function of concentration

confirm the mechanism(s) at play and is beyond the scope of this work.

A complete characterization of f_{NO2} and the amount of HONO in the fully modified chamber was determined under a range of environmentally relevant RHs and NO₂ concentrations. We found that the absolute and fractional NO₂ losses were highest under the highest RH conditions (85%; Table 2). However, the f_{NO2} does not appear to follow a concentration-dependent trend across the additions made at lower RHs, with at most 0.4 ppbv NO₂ lost across the remainder of the tests, a value which is equivalent to the LOD of the NO_x analyzer used. This would generate 0.2 ppbv of HONO according to the disproportionation of the hydrolysis mechanism, which is well below the analyzer detection limits. Overall, the modifications successfully reduce NO₂ losses below 10% across all environmentally relevant conditions the chambers are expected to encounter, with our findings here suggesting that the mass lost is nearly constant and independent of NO₂ mixing ratio at RHs below 85%, while being marginally higher at and above this value.

Quantifying f_{NO2} and the amount of HONO made in the chamber is required for the correction of field datasets. Quantifying NO₂ loss to the chamber surfaces allows us to prevent bias when



742

743

744

745

746747

748

749 750

751 752

753

772



reporting NO₂ exchange processes on environmental surfaces, as the magnitude of the losses attributed to chamber surfaces versus the surface studied can be corrected. The system, via the reference chamber, can also quantify any changes in these processes over time if standard concentration additions to the headspace are conducted. Consequently, important parameters such as NO₂ deposition fluxes on surfaces can be better estimated (Pape et al., 2009).

Since the inferred HONO mixing ratios from the chamber surfaces across various environmental RHs are nearly invariant at 0.2 ± 0.1 ppbv, it is simple to background correct any observational datasets by subtracting this amount from the total HONO measured in the chamber if a more sensitive analyzer is used during field or lab experiments. In addition, as the NO₂ values expected in most atmospheric gas samples during field measurements are well into the ppbv range (>3.3 ppbv per 30-minute flux measurement for a 1.4 ng m⁻² min⁻¹ emission), the corrections would be easy to implement in post-processing of datasets and have minimal impact on the technical aspects of the analytical determinations.

Table 2. Characterization of NO_2 lost in the modified chamber under environmentally relevant ranges of NO_2 and RH. The loss fraction (f_{NO2}) and HONO produced in the chamber were quantified at each of three NO_2 mixing ratios (5, 7, 10 ppbv) delivered at varying relative humidities (RH) to the fully modified chamber. Variability (\pm) provided is one standard deviation of the mean from replicate experiments (n=3).

754 755 756	RH (%)	NO ₂ added (ppbv)	NO ₂ lost (ppbv)	f _{NO2}	HONO produced (ppbv)
757	85	5	0.50 ± 0.01	0.1 ± 0.02	
758 759	85	7	0.70 ± 0.04	0.1 ± 0.02	
760 761	85	10	0.50 ± 0.07	0.05 ± 0.01	
762	65	5	0.30 ± 0.10	0.06 ± 0.02	
763 764	65	7	0.40 ± 0.09	0.06 ± 0.02	<1.1ª
765 766	65	10	0.30 ± 0.08	0.03 ± 0.01	
767	45	5	0.30 ± 0.05	0.05 ± 0.01	
768 769	45	7	0.40 ± 0.04	0.06 ± 0.00	
770 771	45	10	0.30 ± 0.08	0.03 ± 0.01	

^a – below instrument detection limit of 1.1 ppbv determined as S/N=3 while sampling zero air



777

778

780

781

782

783

788

791

792

793

798

800

801

802



773 It should be noted that the amount of HONO in the chamber was below the LOD of the NO_x

analyzer for HONO (1.07 ppbv), meaning that the upper limit of HONO inferred may perhaps, in

fact, be negligible. Therefore, future experiments that wish to detect small N_r fluxes accurately

will need to focus on reproducing these experiments with a higher performance instrument, such

as a time-of-flight chemical ionization mass spectrometer (ToF-MS) or long-path absorption

photometer (LOPAP), which have lower detection limits (Crilley et al., 2019; Lee et al., 2014;

779 Neuman et al., 2016; Reed et al., 2016).

3.2.3 Characterization of O₃ loss in the chamber modified with and without PFA

Ozone loss was observed in both modified and unmodified chamber configurations, with 18% lost

to clean lines alone when transferring 30 ppbv. The unmodified chambers lost 45% across all

delivered mixing ratios (150-250 ppbv), which are higher than those typically expected in ambient

784 air. This was reduced to 35% when the fluoropolymer modifications were implemented with new

clean PTFE fittings and PFA film. When the PFA film was aged by 15 days of ambient sampling

786 and 2 years of exposure to lab air, the losses were substantially exacerbated, reaching 80%. Such

787 outcomes are expected and can be attributed to several factors, primarily involving surface

reactions with built-up films of deposited organics, adsorption, and material interactions

789 (Burkholder et al., 2015).

Ozone is known to undergo heterogeneous surface reactions, particularly on materials like glass,

metals, or polymers (Plake et al., 2015). These surfaces often contain reactive sites such as

hydroxyl groups or adsorbed water molecules that can catalyze the decomposition of O₃ into

molecular oxygen (O₂) and other byproducts (George et al., 2015). Adsorption of O₃ on chamber

surfaces is another potential pathway for loss. When O₃ molecules interact with surfaces, they may

undergo a reaction if the materials are not inert. The use of PFA here was intended to benefit the

796 transfer of O₃, yet despite its high chemical inertness, low reactivity, and resistance to the uptake

797 of many chemicals from gas samples, the subsequent O₃-driven surface reactions are still

substantial (Ebnesajjad, 2017). This is likely because, over time, reactive substances from sampled

799 air accumulated through adsorption on the PFA film and/or its defect sites, thereby reducing its

effectiveness. The same issue is well-known for PFA tubing used in standard air quality monitoring

and is a common maintenance need for O₃ analyzer inlets. Further, physical wear or surface aging

might alter the material surface through product formation or exposure of new reaction sites, which





makes it less resistant to further reaction with O_3 , and therefore increases the rate of loss over time. This is the case in our aged PFA film results, which emphasizes the importance of regular replacement of the film as part of the N_r system maintenance and that quality control procedures characterizing the chamber material performance with respect to O_3 will provide the highest accuracy of experimental results.

808 809

821

822823

824

825

826

827

828

829830

831

807

803804

805 806

3.3 Proof-of-concept reactive nitrogen fluxes using soil samples in the lab

Proof-of-concept flux measurements were performed using the modified dynamic chamber system to demonstrate that emissions of N_r gases from agricultural soil samples can be measured under controlled conditions, similar to many prior reports using custom-built soil chambers (Almand-Hunter et al., 2015; Pape et al., 2009; Tang et al., 2019, 2020).

3.3.1. Fluxes of NO, NO₂, and HONO from agricultural soil samples

Emission fluxes were measured from two pooled and two individual soil samples collected from a single agricultural field (Table 3; Section S6). The average and integrated fluxes of N₂O, NH₃, NO, NO₂, and HONO were assessed under controlled, environmentally realistic, drying conditions of zero air modified to be 65% RH delivered at 3.6 L min⁻¹ to the chamber headspace where the soil was contained. The soil started the drying process from a VWC of approximately 25% with the flows held constant for around 4 days or until the VWC reached 15% (Table 3).

As the soils dried, NO and NO₂ emissions increased, with NO fluxes highest across all replicates and reaching up to 2.50 μ g N m⁻² hr⁻¹. This trend is consistent with the prior work of other researchers, showing peak NO emission potentials when VWC drops below 25% during soil drying, which is when microbial nitrification and denitrification processes are suggested to become more active (Bao et al., 2022; Oswald et al., 2013). The soil VWC at which these maxima occur can vary depending on soil type, texture, and the microbial diversity therein (Ludwig et al., 2001; Schindlbacher et al., 2009). The plot-level replicates from our field had a higher integrated NO flux (i.e., > 2600 μ g N m⁻²), compared to the pooled replicates (<1000 μ g N m⁻²), likely indicating real differences in preserved microbial hotspots, intact plot-level soil aggregates, true spatial variability, and plot-specific N availability (Table 3). Soil texture and aggregate size, for example, play an important role in building the porous structure of soil, which has implications for the





release of gases (Mangalassery et al., 2013). Soil aggregates, therefore, govern the release of 832 833 gaseous N_r analytes like NO based on the aerobic or anaerobic state of the soil. Here, our low level 834 of soil manipulation (i.e. not ground, no sieving) will drive some of the variability by preserving 835 these features, which exist across and within real soil systems (Lipiec et al., 2007). Individual plot 836 samples also retain plot-specific microbial communities when working with intact soil, whereas 837 soil grinding can temporarily inhibit microbial activity. While we tried to minimize soil handling 838 and processing extremes in these experiments, a measure of homogeneity was also pursued, and 839 fully intact soil cores were not assessed. 840 Integrated NO₂ fluxes showed the same trend, with more sample-to-sample variability as one 841 pooled replicate (R2) produced over three times the emissions of R1, despite both experiments 842 being conducted across identical moisture content ranges (Table 3). Given the limited studies 843 directly measuring NO₂, such as Purchase et al. (2023), this variability is difficult to interpret and 844 highlights the need for more assessments of its production pathways and controls, which our 845 developed chambers show promise for. 846 The observed average HONO fluxes remained low across all of the samples, ranging from 0.05 to 0.25 µg N m⁻² hr⁻¹ (Table 3). These values are lower by up to an order of magnitude compared to 847 848 those reported in other controlled laboratory studies, where HONO fluxes ranging from 250 ng N m⁻² s⁻¹ to 900 μg N m⁻² hr⁻¹ have been reported (Oswald et al., 2013; Su et al., 2011; Wang et al., 849 850 2021). These discrepancies are concerning, given recent emphasis from the scientific community 851 on the atmospheric impacts of soil-derived HONO on air quality. Here, the results from our 852 agricultural soil samples may reflect the differences in our methodology, such as the soil handling 853 and preparation steps prior to and during experiments. Many prior reports prepare their samples in 854 ways that strongly deviate from real-world conditions (e.g. initial soil drying temperatures above 855 those occurring under ambient conditions, extreme storage conditions, grinding, sieving, use of 856 dry zero air to flush chambers, etc.). Further drivers of variability within the category of heavily altered samples from the literature include pH, NO₂⁻ availability, and NH₄⁺ or NO₃⁻ content, all of 857 858 which are known to influence biotic and abiotic HONO formation pathways (Wu et al., 2019). 859 Our HONO fluxes from the agricultural soil samples studied here are consistent with field observations under ambient conditions, where average emissions have been reported to largely 860 remain below 2 ng N m⁻² s⁻¹ or 7.2 μg N m⁻² hr⁻¹ (Tang et al., 2019; Xue et al., 2024). This does 861

https://doi.org/10.5194/egusphere-2025-4662 Preprint. Discussion started: 22 October 2025 © Author(s) 2025. CC BY 4.0 License.





862 suggest that greater care in sample preparation, and likely also a widely agreed-upon standard procedure, is needed to study soil HONO emissions relevant to atmospheric models. 863 The integrated HONO fluxes for the pooled replicates yielded 185 µg N m⁻² and 146 µg N m⁻², 864 respectively. From the individual sample replicates, which were slightly wetter than the pooled, 865 the integrated HONO fluxes were 690 and 739 µg N m⁻², which was unexpected because the 866 overall moisture regime accessed by the pooled soil experiments was not lower than those from 867 the plot samples. The drier soils would have been expected to yield greater integrated HONO 868 869 emissions (Oswald et al., 2013), yet this was not the case. Additional replicates and experimental 870 controls, while beyond the scope of this study, would allow further attribution of the controls over 871 the observed HONO variability.





875

samples across two soil VWC ranges. Both the average and integrated fluxes were calculated over a constant period within the noted range of soil VWC. Values are reported as mean \pm standard error. Table 3. Average and integrated fluxes of NO, NO₂, and HONO (in μg N m⁻² hr⁻¹ and μg N m⁻², respectively) from agricultural soil

sample Pooled R1	Range (%) (hr) 16-22 125	(hr)	NO 1.0 ± 0.04	$\frac{\text{NO}_2}{\text{NO}_2}$ H $\frac{\text{H}}{\text{O}_2}$ 0.00	ONO 5 ± 0.02	NO 2400 ± 120	NO_2 HONO 160 ± 50 190 ± 50	HONO 190 ± 50
Pooled R2	16-22	125	1.0 ± 0.04	0.20 ± 0.02	0.05 ± 0.01	2500 ± 130	500 ± 60	150 ± 40
Plot R1	22-27	65	1.2 ± 0.05	1.2 ± 0.05 0.40 ± 0.03	0.20 ± 0.02	3400 ± 150	1300 ± 90 690 ± 70	690 ±
Plot R2	22-27	65	$1.0\ \pm0.03$	$1.0 \pm 0.03 0.50 \pm 0.04$	0.30 ± 0.02	2600 ± 100	1600 ± 100 740 ± 50	740 ±





876 These findings demonstrate the utility of the modified custom-built dynamic chambers for 877 accurately capturing N_r fluxes under controlled laboratory settings, but they also highlight the need for more such systems to be implemented across the scientific community to better consider both 878 879 biogeochemical soil properties and environmental context when interpreting the impacts of N_r 880 fluxes obtained in the lab and scaling them to real soils. There seems to be potential for skewing 881 the atmospheric impacts as a result, in particular for HONO, as the standard approaches have been 882 designed to replicate NO fluxes (Behrendt et al., 2014). Most global models do not consider the 883 effect of soil HONO on air quality through O₃ production and oxidation chemistry (Ha et al., 2023). 884 Several modelling studies like Ha et al. (2023) and Tian et al. (2024) have incorporated the order 885 of magnitude or higher HONO fluxes reported from lab studies, like those by Su et al. (2011), Wang et al. (2021), Oswald et al. (2013), and Meusel et al. (2018). They estimated significant 886 HONO production with maximum flux potentials of 830 µg N m⁻² hr⁻¹, 95 µg N m⁻² hr⁻¹, 70 µg N 887 m⁻² hr⁻¹, 55 µg N m⁻² hr⁻¹, respectively. In contrast, the field observations that do exist suggest that 888 real HONO fluxes are much smaller at 2-17.5 µg N m⁻² hr⁻¹ (Song et al., 2023; Tang et al., 2019). 889 Similarly, Wu et al. (2022) has used the regional WRF-Chem model to explore the impact of soil 890 891 HONO emissions on the concentrations of atmospheric HONO, OH, and O₃. Agricultural soil HONO emissions have been suggested to significantly contribute to OH radical 892 893 production, accounting for approximately 10% to 60% of total OH formation in rural areas before 894 noon (Oswald et al., 2013; Su et al., 2011), which often exceed the contributions from ozone 895 photolysis. Additionally, high HONO emissions from agricultural soils have been reported to 896 increase local O₃ concentrations by ~0.5 - 1.0 ppb in low-NO_x rural environments where VOCs 897 are not limiting (Zhang et al., 2021), with even greater impacts observed during fertilization 898 periods (Wu et al., 2022). Modelling studies, using GEOS-Chem and CMAQ, for example, claim 899 that incorporating soil HONO emissions improves the agreement between observed and simulated 900 O₃ levels, particularly during the morning (Zhang et al., 2021). 901 Only a few studies have conducted estimates of soil NO_x emissions under reasonable conditions, 902 like Bao et al. (2022) and Wu et al. (2022), where the researchers tried to mimic field conditions. 903 Even in such an area that has been long studied, large uncertainty still exists around soil sources 904 of NO_x, particularly for agricultural activities where uncertainty is still at least ±30% due to 905 limitations in lab characterizations and field experiments (Gong et al., 2025). It is not surprising,



907

908

909

910

911

912

913

914



then, that a similar issue exists for the very recent work on HONO soil emissions. The NO_x uncertainty range results from intricate soil biogeochemical processes and varies with crop types, soil texture, fertilizer types and application rate (Gong et al., 2025). This longstanding and established difficulty in predicting soil NO_x for use in global chemical models means that doing so for HONO without careful ground truthing of real-world emissions could lead to substantial inflation of the impacts on atmospheric chemistry and air quality. Care should be taken in using HONO emissions from lab studies in global models, as it seems they pose a risk of overestimating their atmospheric impacts until a more representative experimental design can be obtained with chamber systems like the one used here.

915 916

917

918

919

920

921

922

923

924

925

926

927

928

929

930

931

932

933

934

3.3.2 Fluxes of NH₃, N₂O, NO, NO₂, and HONO from fertilized agricultural soil samples

Agricultural soils amended with chemical fertilizers are expected to be hotspots for NH₃, N₂O, HONO, and NO_x emissions. Here, we demonstrate the use of our developed chambers to measure these analytes under controlled lab conditions using our lightly processed pooled soil samples and four fertilizers: urea, ammonium nitrate (AN), ammonium bicarbonate (ABC), and ammonium carbonate (AC) with the temperature maintained at 23 °C, VWC between 25–29%, and headspace RH held at 65% for three days, simulating realistic atmospheric and environmental N_r flux exchange conditions following farm field fertilization (Figure 3). In all experiments conducted with the Picarro G2509, the mixing ratio of N₂O began to rise approximately four hours after the experiment started. In the example shown for urea, it peaked at 0.79 ppm after 12 hours, which was followed by a gradual decline (Figure 3a). This pattern likely reflects the incubation period of nitrifying and denitrifying bacteria that leads to the subsequent release of gases like HONO, as depicted in Wang et al. (2021), and N₂O in Liu et al. (2022). In contrast, the mixing ratio of NO remained relatively constant throughout the three days (Figure 3b), with NO2 increasing as the N₂O emissions decreased, while NO was emitted constantly throughout (Figure 3c). In this example experiment, no measurable emissions of HONO were detected despite the substantial presence of urea and evidence of active microbial nitrification and denitrification from the other emitted gases (Figure 3d). Lastly, the urea application example in Figure 3e shows the expected significant NH₃ emissions, with the integrated amount reaching 22% of the applied N over the





three-day incubation period. These findings are consistent with our existing knowledge that NH_3 volatilization as an N loss mechanism dominates early N_r losses from fertilizers.

Volatilization of NH₃ is well-characterized as a major pathway for N loss from fertilizers (Behera et al., 2013; Govoni Brondi et al., 2024; Liu et al., 2020; Moravek et al., 2019; Pan et al., 2016, 2022; Paulot et al., 2014). Besides agronomic concerns due to N loss and reduced fertilizer efficiency related to NH₃ emissions from fertilized soil (Anas et al., 2020), it is a key precursor to secondary inorganic aerosols in the atmosphere with impacts on respiratory and ecosystem health, visibility, and climate (Dennis et al., 2010; Edwards et al., 2024; Fowler et al., 2013; González Ortiz et al., 2020; Jang et al., 2025; Seinfeld and Pandis, 2006).

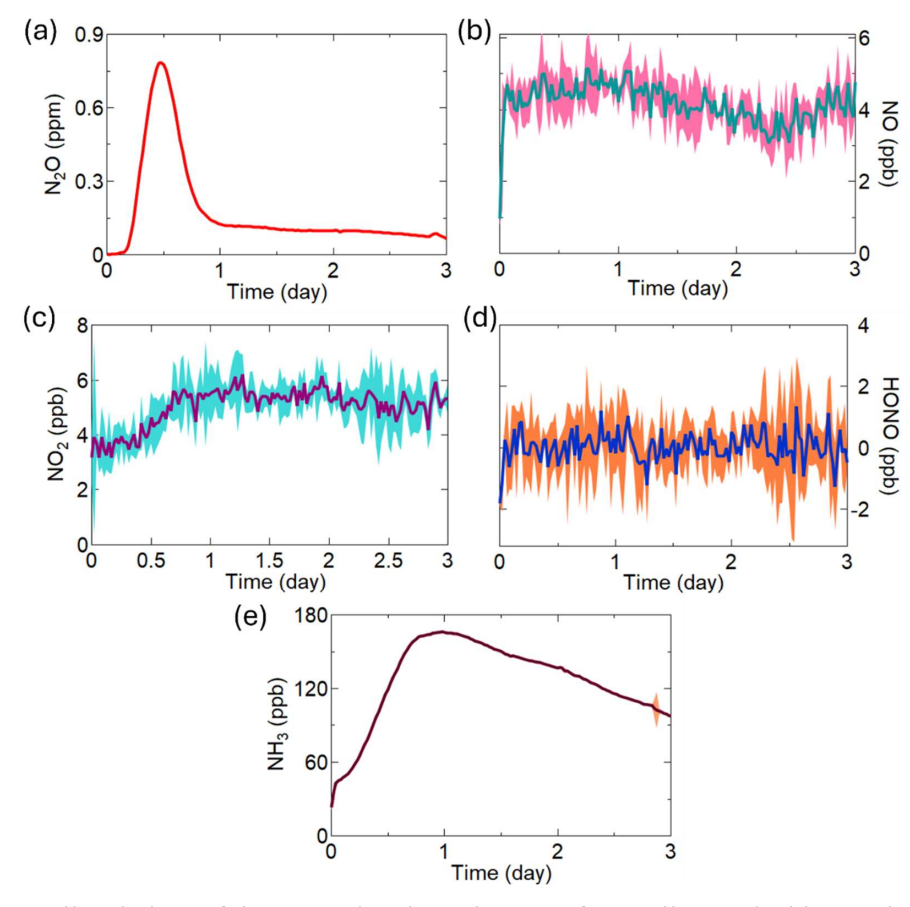


Figure 3. Soil emissions of the comprehensive suite gases from soil treated with urea, including (a) N_2O ; (b) NO; (c) NO_2 ; (d) HONO; and (e) NH_3 . The NO, NO_2 and HONO emissions were measured at 1-minute resolution and averaged to 30 min. The standard deviation ($\pm 2\sigma$) around these averages is shaded with a lighter version of the main trace colour. Similarly, the 2-second



950

958

959

960 961

962

963 964

965

966

967

968 969

970

971

972

973

974

975

976 977



resolution of N₂O and NH₃ measurements were also averaged to 30-minute intervals with $\pm 1\sigma$ provided in shading.

951 Emissions of NH₃ and N₂O were observed to be far greater in terms of integrated amounts from 952 953 954 955 956 957

the fertilized samples (Figure 4). Integrated flux for NH₃ produced by soil treated with ABC accounted for 77% of total N_r flux (i.e., 85900 µg N m⁻²), followed by AC, which was 63700 µg N m⁻². This is not surprising, since the use of chemical fertilizers increases the concentration of NH₄ in the soil that can deprotonate to emit neutral NH₃ and, in the presence of ammoniaoxidizing microorganisms, increases the production of N2O (Luo et al., 2025). Nitrous oxide released from the addition of urea accounted for the highest integrated flux of 32400 µg N m⁻² observed, representing 89% of total N_r released, followed by 25300 µg N m⁻² and 9600 µg N m⁻² for ABC and AC, respectively. One way that has been proposed to reduce these large N₂O emissions from inorganic fertilizers is to change the application form to organic fertilizer, as the NH₄⁺ in soil is released more slowly (Luo et al., 2025). Due to a limited duration of access to the G2509 to conduct this work, we were unable to measure the N2O and NH3 emitted from unamended soils or those treated with AN. Regardless, based on the obtained data, the values found here are similar to those observed under real environmental conditions (Figure 4). For our sample without N amendment, the integrated flux of NO was the largest (2400 µg N m⁻²; 87% of total NO_v), followed by comparable levels of NO₂ (160 µg N m⁻²) and HONO (190 µg N m⁻²). The fluxes of NO_x and HONO were below 1 $\mu g \ N \ m^{-2} \ hr^{-1}$ for all the nutrient addition treatments, suggesting a similar trend as those observed under field conditions and from our lab results with unamended soils (Figure 4, Table S1, Section S6). The exact mechanism behind the HONO release, being due to nitrification and/or denitrification, cannot be definitively assigned based on flux data alone, and many abiotic factors like soil moisture, temperature, and presence of specific microbial communities drive these emissions. There are discrepancies still observed between HONO flux measured from the treated soil samples in the laboratory and similar measurements in literature (Oswald et al., 2013; Su et al., 2011), some of which report fluxes of up to ~3600 µg N m⁻² hr⁻¹ and are likely overestimating the soil N_r fluxes found in the real world. In contrast, our results are in close agreement with the field-based measurements of Tang et al. (2020), which also used a dynamic chamber flux method.

978 979





These in-lab experiments show that simultaneous speciated N_r emissions in a controlled environment can be conducted using a single chamber and potentially applied to an array of chambers, as others have done for a subset of gaseous N_r (Scharko et al., 2015; Tang et al., 2019). With even limited replicates we did here, our results raise a question for researchers who have been using lab studies as a standard to predict and incorporate HONO soil emission values in particular, into regional and global models.

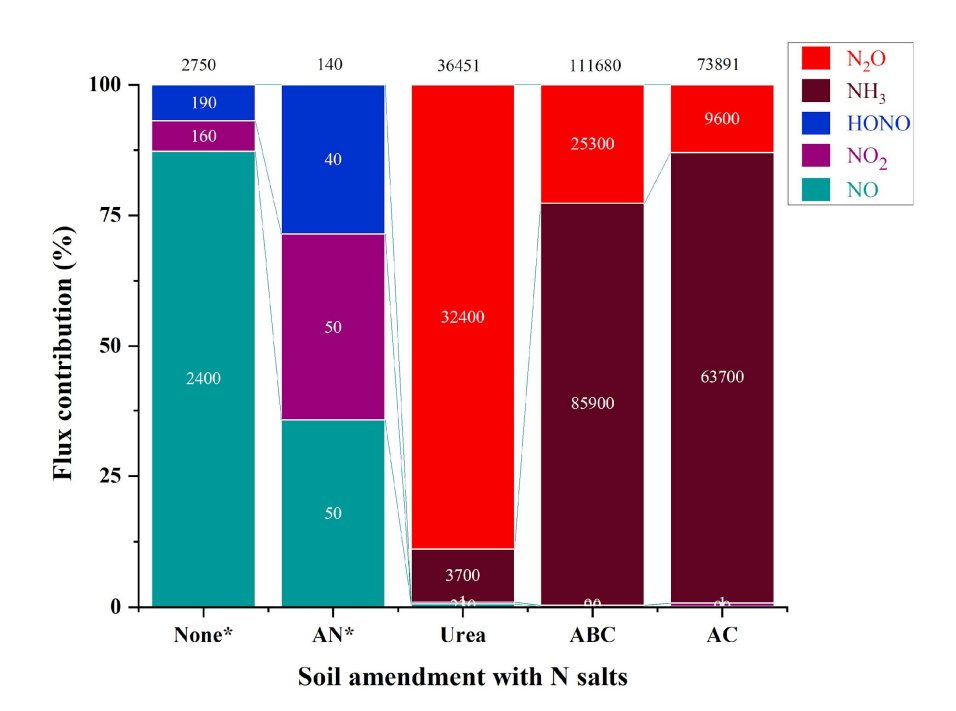


Figure 4. Relative flux contribution of soil treated with four different nitrogen-containing fertilizer salts. Each segment shows the proportion of integrated flux of NO (cyan), NO₂ (purple), HONO (blue), NH₃ (brown) and N₂O (red), with discrete flux values presented in white text, and the total flux provided in black text above the column (μ g N m⁻²). Some samples (denoted by *) were only characterized for fluxes of NO, NO₂ and HONO using the modified NO_x analyzer, as the duration of our access to the G2509 for NH₃ and N₂O measurements was limited.

3.3.3 Dual chamber field deployment for automated continuous dynamic fluxes

A pilot scale field campaign was carried out to demonstrate the application of our dual soil flux chambers in capturing N_r gas exchange processes, taking into account the characterized processes presented above that are necessary for accurate determinations. A paired measurement and reference chamber setup was deployed in the same field a year after the soil samples were collected





for our lab experiments. During a period of stimulated N_r emission from an experimental application of urea in situ, the mixing ratios of NO, N_2O , and NH_3 were impacted compared to the unfertilized state. The changes within both the measurement and reference chambers were measured and used to calculate fluxes (Figure 5). The selected data for NH_3 correspond to measurements taken after the fertilization event, while the selected NO and N_2O data segments are examples prior to the fertilization event so that the mathematical terms in E6 and E7 contributing to the net flux can be considered more easily – they are entirely ascribed to the rate term otherwise. Each set of observations span three consecutive hours of dynamic changes in gas concentrations within the chambers which allow fluxes to be calculated.

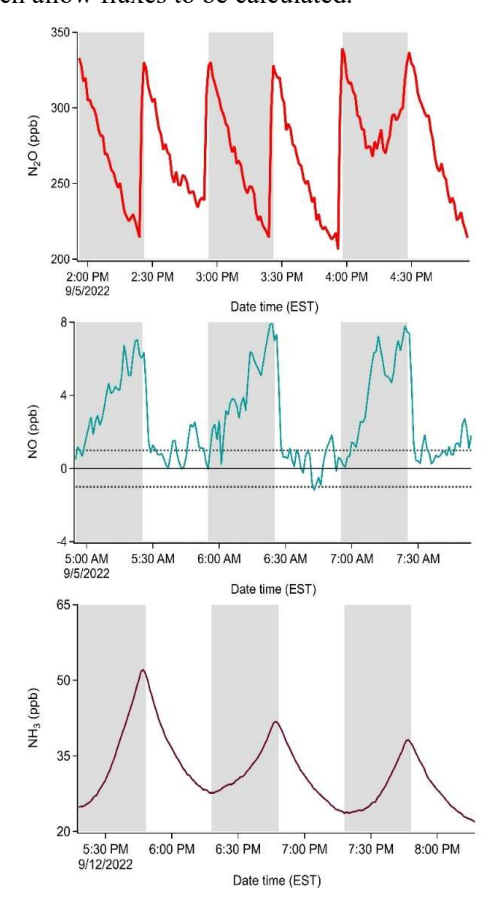


Figure 5. Mixing ratios of N₂O (ppb), NO (ppb), and NH₃ (ppb) in the measurement (grey shading) and reference (unshaded) chambers from three consecutive cycles during the pilot field study. The NH₃ cycles correspond to measurements taken after the fertilization perturbation, while the NO





and N₂O cycles are from the same period before fertilization. The dashed lines for the NO 1012 measurements indicate ± 1 ppb (3 σ noise), where the positive boundary represents the detection 1013 1014 limit of the NO_x analyzer. 1015 The breakdown of the flux components for NH₃, N₂O, and NO can allow the contributions of the 1016 experimental setup (e.g. dilution) and environmental factors (e.g. reaction) to be considered 1017 independently (Figure 6). We consider these across three consecutive measurement cycles from 1018 the pilot field deployment, to provide meaningful examples. The uncertainty in each term is 1019 estimated from a triplicate of consecutive reference chamber background measurements. 1020 Therefore, the error bars for each term are derived from the variability in the measured slope of 1021 the three reference chamber measurements. This error estimate corresponds to that arising only 1022 from reference chamber observations used in E6 or E7 and assumes that ambient atmospheric 1023 composition did not change substantially during this error derivation period. 1024 The rate term (dC/dt) is the dominant contributor to the determined flux for all three gases (Figure 1025 6), which are all positive and indicate emissions despite their clearly differing temporal trends. 1026 Each contribution term is defined and discussed in further detail in Section S7 of the 1027 Supplementary Information. Accurate quantification of trace gas fluxes using dynamic chamber 1028 systems requires correction for attenuation caused by surface interactions. These effects can significantly suppress the measured accumulation rate of reactive species within the closed 1029 chamber, particularly for compounds with notable surface affinities such as NH₃, NO₂, and HONO 1030 1031 (Figure 5). To account for such losses, an attenuation factor (λ) was introduced in this work (ES12), 1032 defined as the ratio of the theoretical concentration signal to the measured signal over the chamber closure period. The value of λ is gas-specific and time-dependent, reflecting wall affinity and 1033 1034 kinetics, which are therefore calculated over the first 30 min of chamber closure, as this was the duration of our field measurement closures. This correction reduces bias that would otherwise 1035 1036 result in the calculated gas exchange rates, independent of chamber-specific losses. The highest 1037 attenuation was observed for NH₃, for which a λ of 5.40 was determined for the corresponding 1038 closure period. That is, substantial bias would result without this correction. Comparative values

for NO₂ and HONO are also provided in the Supporting Information (Section S7.3).



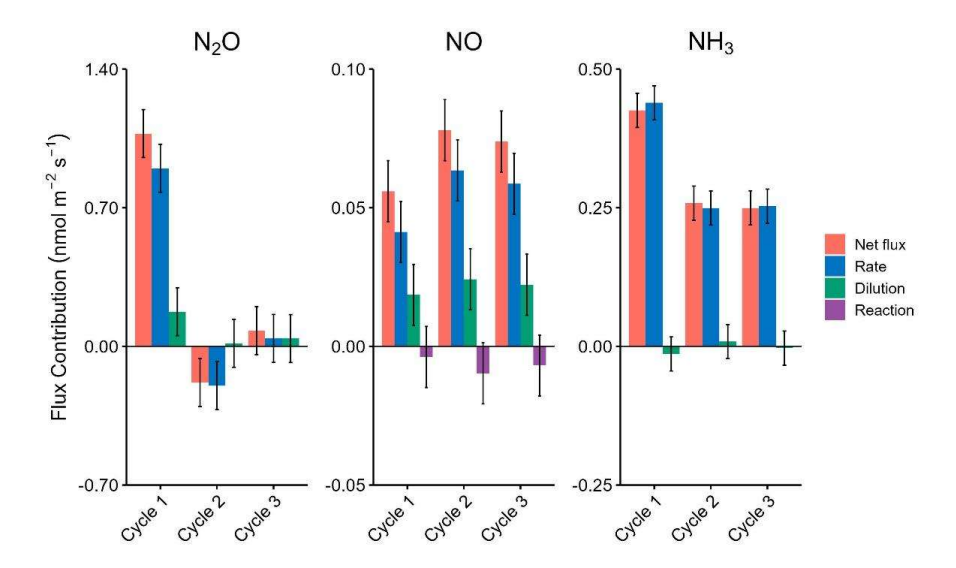


Figure 6. Contributions of different terms (rate, dilution, and reaction) to the net flux of NO, NH₃, and N₂O across three consecutive cycles (nmol m⁻² s⁻¹). The rate represents the change in concentration measured over time, the dilution represents the integrated loss to dilution, and the reaction represents the contribution of known reactions happening inside the chamber. Error bars are calculated using the mean value of the corresponding terms from three reference chambers plus their standard deviation. For visual clarity, the attenuation correction ($\lambda = 5.40$) for NH₃ is not applied in this figure, as it constitutes a linear scaling factor across all NH₃ bars (Section S7.3).

For N_2O , the first cycle exhibits the highest flux $(1.07\pm0.12 \text{ nmol m}^{-2} \text{ s}^{-1})$, while the second cycle showed uptake by the soil $(-0.18\pm0.12 \text{ nmol m}^{-2} \text{ s}^{-1})$, and the final cycle showed no net flux within error $(0.08\pm0.12 \text{ nmol m}^{-2} \text{ s}^{-1})$. This occurs for a non-reactive greenhouse gas like N_2O despite the concentration decreasing with time for both the measurement and reference periods, as the rate of decrease during the measurement cycle is slower than that from dilution alone (Figure 6). Across the three cycles, the rate of concentration change term contributed $84\pm15\%$ to the measured flux in the first cycle, $109\pm98\%$ in the second cycle, and $50\pm171\%$ in the third cycle. The negative rate of change in all of the observation periods arises due to the use of N_2O -free purge gas delivered to the chamber headspace, which is required for the gas sample to be destructively quantified, while not introducing ambient air into the chamber. This simultaneously prevents sudden changes in local outdoor air composition from making small fluxes difficult to detect, as well as reduces the uncertainty in the fluxes assigned. Here, the dilution terms range from 8 to 50% of the net flux, as would be expected from the N_2O exchange switching from emission to deposition during the three-



1062

10631064

1065

1066

1067

1068

10691070

1071

10721073

1074

10751076

1077

1078

1079

1080

1081 1082

1083

1084

10851086

1087

1088

1089 1090

1091



transitions from a loss to steady state during the observation period, suggesting that an instant of 'hot spot, hot moment' emission of N₂O was likely occurring. As such, the transition leads to no net flux for the observation period, which is a limitation of our dual-chamber approach compared to one with recirculating headspace, or that of an eddy covariance approach that can capture much higher temporal resolution changes in concentration. The N2O fluxes observed here are consistent with those reported for European arable soils using both dynamic and static chambers, where event-driven N₂O peaks after fertilization commonly range between 0.2 and 2.4 nmol m⁻² s⁻¹, and background periods can be as low as 0.08 nmol m⁻² s⁻¹ (Kong et al., 2025, Murphy et al., 2022, Maier et al., 2024). Field-scale eddy covariance studies, such as Maier et al. (2022), have captured post-harvest pulses up to 1.6 nmol m⁻² s⁻¹, highlighting the capacity of EC to resolve large, rapid emission events that single-point chamber systems may miss. However, dynamic chamber systems provide high-precision, temporally resolved flux data under controlled conditions, enabling direct attribution of emissions to specific soil management or environmental factors (Butterbach-Bahl et al., 2013; Kong et al., 2025). This makes dynamic chambers, like those demonstrated here, especially valuable for mechanistic and process-level studies. For NO, the only gas we consider in the examples here with a reaction term, the reaction contribution is the smallest among the three flux components. Over all three cycles, the reaction term opposed the net flux by less than 13%. The magnitude of the reaction term is always negligible, remaining within the ± 0.01 nmol m⁻² s⁻¹ variability caused by background correction from the reference chamber. Instead, the time rate of change in concentration term drove 74-81% of the total flux for all three cycles and dilution accounted for the remaining 30–33%. The reaction term falling within the uncertainty range of no contribution in all three cycles (e.g. -0.01±0.01 nmol m⁻² s⁻¹ in the second cycle, where it had the greatest potential), indicates that its contribution is less certain than the other flux components as it is driven by the presence of O₃, which is rapidly lost upon chamber closure. Overall, the low contribution of the reaction term suggests this process has a minor role in measured NO fluxes. In other, more polluted regions, such as the North China Plain (NCP) and the Pearl River Delta (PRD), where summertime ambient O₃ concentrations frequently range from 60 to 275 ppby, and exceedances above 200 ppby occur during pollution episodes (Wang et al., 2017), this term could become very important to include. As noted above, the PFA film on the chamber surface will change its properties with respect to O₃ transmission

cycle example (i.e. 3 hours). In the final measurement cycle, the rate of concentration change





1092 over time, highlighting the utility of the reference chamber, which is designed to accumulate the 1093 same atmospheric compounds as the measurement chamber over time on all sampling surfaces. The resulting emission fluxes of NO observed in these three cycles were 0.056-0.078 nmol m⁻² s⁻¹ 1094 1095 1, which is well within the range reported for agricultural soils in North America and Europe, such as Taylor et al. (1999) who observed -0.07-4.2 nmol m⁻² s⁻¹ in Canadian fertilized cropland, and 1096 Pape et al. (2009) and Almand-Hunter et al. (2014) who reported values of 0.05-4.0 nmol m⁻² s⁻¹, 1097 using dynamic chambers in grass and cropland soils. Therefore, in the case of NO for this example, 1098 1099 the variability in the fluxes is largely driven by real fluctuations in the rate term. This highlights 1100 the sensitivity of the total flux to changes in the rate of concentration change, and the precision of 1101 the method, as the uncertainty in the final fluxes here is on the order of 14%. Compared to the dynamic chambers reported by these prior studies, our reference chamber in our dual-chamber 1102 1103 system offers a clear advantage by directly correcting for baseline fluctuations and environmental drift that can confound single-chamber approaches. This is especially important for reactive gases 1104 1105 such as NO, which are susceptible to rapid loss to O3 and short-term background variability (Taylor 1106 et al., 1999). The dual-chamber system provides more robust, artifact-free quantification of soil-1107 atmosphere exchange and is less susceptible to interference from transient local emissions (e.g. 1108 from nearby traffic or agricultural equipment) than single-chamber systems. In comparison to eddy 1109 covariance or flux-gradient techniques, which integrate over larger areas but may underestimate 1110 true NO fluxes due to post-emission chemistry (Taylor et al., 1999; Plake et al., 2015), our 1111 approach yields high-frequency, process-resolving data ideal for mechanistic and plot-scale 1112 studies. For NH₃, the rate of change term dominates the total flux, contributing $103 \pm 10\%$, $97 \pm 16\%$, and 1113 $101 \pm 17\%$ of the flux in cycles one, two, and three, respectively, while the dilution term 1114 1115 contributes inconsequentially at $-3 \pm 7\%$, $3 \pm 12\%$, and $-1 \pm 12\%$ in the same three cycles, 1116 respectively. The resulting emission fluxes of NH₃ observed across these cycles ranged from 0.43 ± 0.03 nmol m⁻² s⁻¹ in cycle one down to 0.25 ± 0.03 nmol m⁻² s⁻¹ in cycle three. The relatively 1117 1118 small contribution of the dilution term is consistent with the expectation that the reference and 1119 measurement chambers exhibit similar dilution effects. The relative uncertainty in the final NH₃ 1120 fluxes is 7% for cycle one, and 12% for cycles two and three. By comparison, relative uncertainties



11231124

1125

1126

1127

11281129

1130

11311132

1133

1134

1135

1136

11371138

1139

1140

1141

1142

1143

1144

1145

1146

1147

1148

1149

1150



were 14% for NO and ranged from 15% to 171% for N₂O, reflecting the greater variability and lower precision associated with the smaller flux magnitudes for those gases.

Our observed NH₃ fluxes (0.25–0.43 nmol m⁻² s⁻¹) are consistent with literature values for managed grass and croplands. For instance, Milford et al. (2009) reported bi-directional background fluxes from -3.8 to 2.5 nmol m⁻² s⁻¹ prior to cutting intensively managed grassland, with larger diurnal emissions up to 42 nmol m⁻² s⁻¹ after cutting and maxima up to 224 nmol m⁻² s⁻¹ following fertilizer application. Abdulwahab et al. (2024) observed highly variable fluxes in intensively grazed French grassland, ranging from -6.6 to 188 nmol m⁻² s⁻¹, with short-lived maxima above 300 nmol m⁻² s⁻¹ after slurry application, though most measurements were at much lower magnitudes. Notably, accurate quantification of NH₃ fluxes in this system critically depends on the application of the chamber-specific attenuation factor λ (Section S.7.3). In our study, λ for NH₃ was 5.40 for the 30minute closure interval, meaning that without this correction, true NH3 fluxes would be underestimated by more than fivefold. The necessity of such a large λ correction is due to the strong surface affinity of NH₃ and emphasizes the importance of it for gas- and chamber-specific corrections to obtain high-quality N_r fluxes. While the reference chamber correction plays a role in the flux calculations, its impact on NH₃ is less pronounced than on N₂O, where the correction significantly alters the net flux direction (Figure 5; first cycle). Chamber-based approaches such as ours provide a key advantage for NH₃ over micrometeorological methods like eddy covariance, which are especially prone to high-frequency attenuation and chemical interferences for reactive gases. As shown in Moravek et al. (2019), even state-of-the-art closed-path EC systems may recover less than half (as little as 46%) of true NH₃ fluxes due to instrument limitations and turbulence losses. Challenges were also evident for relaxed eddy accumulation (REA), where Xu et al. (2010) found that turbulence and surface effects complicated flux interpretation in cropland. Related methodological considerations have also been noted in other contexts. Schlossberg et al. (2017) highlighted how airflow and canopy structure can influence chamber NH₃ fluxes in turf systems, underscoring the need for chamber methods that minimize such artifacts. In contrast, our dynamic chamber system, with a chamber-specific λ correction and reference chamber, enables robust, bias-corrected quantification of both low and episodic NH3 fluxes, as well as clear partitioning of emission and dilution terms, even under highly variable field conditions. Overall, the combination of dual-chamber design with explicit λ correction in our method provides more

4. Conclusions



1151

1152

1153

1177

1178

1179

1180



1154 In this work, we presented a dynamic chamber system for reactive nitrogen flux measurements, 1155 developed for the first time through the modification of commercially available chambers by 1156 implementing two key changes: the use of PTFE fittings instead of original brass fittings and the 1157 installation of an inert PFA film, which retains their actinic transparency. These modifications 1158 provide a targeted methodology for other researchers to convert commercially available chambers 1159 into those capable of measuring N_r. The performance of these modifications was quantified 1160 through the rise and fall time constants of target gas concentrations, as well as a reduction in 1161 reactive losses. The time constants for the transfer of GHGs were not different from those of a 1162 theoretically inert gas and showed no change from the modifications. Improved transmission for 1163 the reactive and surface-active N_r species NO₂, HONO, and NH₃ targeted here ranged from 0.8 to 2.6 minutes. Similarly, a commercial chamber multiplexing unit with stainless steel valves and 1164 fittings replaced with PTFE and PFA, respectively, resulted in a 9-27% reduction in surface losses 1165 1166 of N_r compounds. 1167 Only NO₂ showed reactive loss in the system, and the loss fraction in the chambers in their

accurate and robust quantification of soil NH₃ emissions than single-chamber, eddy covariance, or

relaxed eddy accumulation techniques, particularly for short-term or low-flux events.

1168 unmodified configurations was up to ~36%. Losses were reduced to the gas analyzer detection 1169 limits (<10%) with the same fluoropolymer modifications when atmospherically relevant NO₂ and 1170 RH mixtures were introduced. Lastly, O₃ loss was pervasive within chambers in both their 1171 modified and unmodified configurations at 35% and 45% respectively, demonstrating the 1172 necessity of the reference chamber. It allows characterization of deposited surface film reactivity 1173 for O₃, especially when obtaining quality O₃ measurements is needed to account for the conversion of NO to NO₂ during a sampling period. Taken together, the modified commercial system is 1174 1175 capable of measuring dynamic soil fluxes of GHGs and N_r when a measurement and reference 1176 chamber are deployed simultaneously.

Proof of concept flux measurements using this N_r dynamic chamber system were conducted using real agricultural soil samples in the lab, with a single chamber, and during a pilot study in the field with a measurement-reference chamber pair. The lab soil emissions were found to be consistent with prior field reports in the literature for NO and HONO, with unexpected emissions of NO_2 also





1181 observed. Substantial variability in NO₂ and HONO emissions between replicates demonstrates the potential heterogeneity of soil emissions that may result from samples kept intact and subject 1182 to minimal preparation conditions. Upon the addition of typical fertilizers, like urea, substantial 1183 1184 NH₃ and N₂O emissions fluxes matched expectations, with increasing quantities of NO, NO₂, and 1185 HONO as the soil water content decreased. 1186 Last, fully automated operation of the chambers was carried out in a field pilot study with the 1187 delivery of external fertilizer conducted at the midpoint of the study to stimulate N_r emissions, 1188 mainly in the form of NH₃. Continuous flux observations were made by switching sample flows 1189 between a paired reference and measurement chambers with a custom-built valve system to obtain 1190 continuous N_r fluxes over two weeks. While the details of the entire campaign will be presented 1191 in a future manuscript, it was shown here how the methodology developed yields reliable flux 1192 determinations by accounting for known reactions and our lab-derived surface effects. The 1193 mathematical foundation of each term and its error in a mass balance equation, which are central 1194 to reducing flux bias, are fully described. The observed fluxes from our dynamic chambers are 1195 simpler to quantify with standard gas analyzers and can be compared readily with prior reports in 1196 the literature from other common flux techniques. One key limitation of the dynamic chamber 1197 approach is the limited footprint covered in a system that is notoriously heterogeneous, where EC 1198 and REA flux approaches are less prone to this effect. Using a multiplexer and a larger array of 1199 dynamic chambers, it is possible to reduce the susceptibility of the dynamic chamber approach to 1200 this issue. 1201 Through our modifications and validation, this work provides insight into how commercial 1202 dynamic chamber options, like those offered by Eosense, can be modified easily for scientists from 1203 various disciplines interested in studying N_r exchange at atmospheric interfaces. This is 1204 particularly important for research groups which currently do not have the expertise and resources 1205 to develop their own N_r flux measurement systems. The modified system utilizes destructive 1206 sampling techniques, as opposed to the re-circulation of chamber air, enabling integration of the 1207 dynamic chamber approach with various standard gas analysis instruments (e.g., NO_x 1208 chemiluminescence) to study their exchange. The large footprint allows gas concentrations to 1209 change in easily determined quantities even for very small fluxes. We show here, for the first time, 1210 that such a system can provide simultaneous measurement of NO, NO₂, HONO, NH₃, CO₂, H₂O,





CH₄, and N₂O fluxes. In addition, we show fully automated operation of the chambers, switching 1211 1212 of sample flows, and data collection workflows for continuous and unattended measurements of 1213 fluxes at field sites. Given the pressing need to understand global perturbations to the 1214 biogeochemical cycle of N, reduce nitrogen use in agriculture, and gauge the impacts of N status 1215 on biodiversity or ecosystem function, wider accessibility of N_r flux techniques for the global 1216 research community is needed to increase the pace of research outcomes and improve the capacity 1217 for interdisciplinary work between atmospheric and earth system researchers. 1218 **Data Availability:** Data is available upon request from the Corresponding Author. 1219 Competing Interests: TCV received supporting in-kind funds for this work from Eosense, Inc. 1220 and Picarro as it is mandatory in the NSERC Alliance Missions programme funding structure 1221 which facilitates research partnerships between the academy and industry. NN, CC, and SE are 1222 employed by Eosense, Inc. 1223 Author contributions: TCV designed and oversaw the experiments, acquired funding, wrote parts 1224 of the manuscript, and guided writing and revision of all sections of the manuscript. MS wrote the 1225 manuscript and performed all the lab experiments. KZA carried out the multiplexer experiments, 1226 conducted data analysis for the fill-empty experiment, provided guidance and feedback on the 1227 derivation of the mass balance flux model, and assisted in the revision of the manuscript. DF conducted some of the field measurements, worked up the pilot field study results and derived the 1228 1229 dual chamber mass balance flux calculations, and made contributions to the writing and revision 1230 of the manuscript. LRC helped design the experiments, modify the chambers, write the LabVIEW 1231 code, conduct the pilot field measurements, and contributed to manuscript preparation and 1232 revision. AM contributed to the initial chamber lab setup and revision of the manuscript. FS 1233 performed some fill-empty and NO₂ loss experiments, designed the custom valve switching 1234 system, modified LabVIEW code for the pilot field measurements, and contributed to initial drafts 1235 of the manuscript. YEI and TH assisted with the GHG fill-empty experiments, YEI supported the 1236 pilot field study, and both contributed to manuscript revision. NN, CC, and SE provided technical 1237 support with setting up and modifying the chambers and multiplexer. 1238 Acknowledgements: We gratefully acknowledge the support of Picarro for facilitating use of the

G2509 analyzer during the chamber characterizations, lab experiments, and pilot study

https://doi.org/10.5194/egusphere-2025-4662 Preprint. Discussion started: 22 October 2025 © Author(s) 2025. CC BY 4.0 License.





1240 components of this work. The team at Shawnasey Farms Ltd. provided access to storage and 1241 machinery to install the experimental agricultural site for the pilot project, helped with daily 1242 campaign logistics, and the collection of soil samples. 1243 Financial Support: All components of this work were supported by funding to TCV by the 1244 Natural Sciences and Engineering Research Council (NSERC) Alliance Missions program 1245 (ALLRP 570577-2021), with additional support from the NSERC Discovery Grants and Early 1246 Career Launch programmes (RGPIN-2020-06166 and DGECR-2020-00186). MS and YEI were 1247 supported by Ontario Graduate Scholarships, and MS was further supported by a Charles Hantho 1248 Award in Atmospheric Chemistry and the Enbridge Graduate Student Award.

1249





- 1250 **5. References**
- Almand-Hunter, B. B., Walker, J. T., Masson, N. P., Hafford, L., & Hannigan, M. P. (2015).
- 1252 Development and validation of inexpensive, automated, dynamic flux chambers.
- 1253 Atmospheric Measurement Techniques, 8(1), 267–280. https://doi.org/10.5194/amt-8-267-
- 1254 2015
- 1255 Anas, M., Liao, F., Verma, K. K., Sarwar, M. A., Mahmood, A., Chen, Z. L., Li, Q., Zeng, X. P.,
- 1256 Liu, Y., & Li, Y. R. (2020). Fate of nitrogen in agriculture and environment: agronomic,
- eco-physiological and molecular approaches to improve nitrogen use efficiency. In
- 1258 Biological Research (Vol. 53, Issue 1). BioMed Central Ltd.
- 1259 https://doi.org/10.1186/s40659-020-00312-4
- 1260 Aneja, V. P., Blunden, J., Claiborn, C. S., & Rogers, H. H. (2006). Dynamic Chamber System to
- 1261 Measure Gaseous Compounds Emissions and Atmospheric-Biospheric Interactions.
- 1262 Environmental Simulation Chambers: Application to Atmospheric Chemical Processes, 97–
- 1263 109. https://doi.org/10.1007/1-4020-4232-9_7
- 1264 Anthony, T. L., & Silver, W. L. (2024). Hot spots and hot moments of greenhouse gas emissions
- in agricultural peatlands. *Biogeochemistry*, 167(4), 461–477.
- 1266 https://doi.org/10.1007/s10533-023-01095-y
- Bao, F., Cheng, Y., Kuhn, U., Li, G., Wang, W., Kratz, A. M., Weber, J., Weber, B., Pöschl, U.,
- 1268 & Su, H. (2022). Key Role of Equilibrium HONO Concentration over Soil in Quantifying
- 1269 Soil–Atmosphere HONO Fluxes. *Environmental Science & Technology*.
- 1270 https://doi.org/10.1021/acs.est.1c06716
- 1271 Barney, W. S., & Finlayson-Pitts, B. J. (2000). Enhancement of N2O4 on Porous Glass at Room
- 1272 Temperature: A Key Intermediate in the Heterogeneous Hydrolysis of NO2? *Journal of*
- 1273 *Physical Chemistry A*, 104(2), 171–175. https://doi.org/10.1021/jp993169b
- 1274 Becciolini, V., Leso, L., Fuertes Gimeno, E., Rossi, G., Barbari, M., Dalla Marta, A., Orlandini,
- 1275 S., & Verdi, L. (2024). Nitrogen loss abatement from dairy cow excreta through urine and
- facces separation: The effect of temperature and exposure period on NH3 fluxes.
- 1277 Agricultural Systems, 216. https://doi.org/10.1016/j.agsy.2024.103898
- 1278 Behera, S. N., Sharma, M., Aneja, V. P., & Balasubramanian, R. (2013). Ammonia in the
- 1279 atmosphere: A review on emission sources, atmospheric chemistry and deposition on
- 1280 terrestrial bodies. In Environmental Science and Pollution Research (Vol. 20, Issue 11, pp.
- 1281 8092–8131). https://doi.org/10.1007/s11356-013-2051-9
- Behrendt, T., Veres, P. R., Ashuri, F., Song, G., Flanz, M., Mamtimin, B., Bruse, M., Williams,
- 1283 J., & Meixner, F. X. (2014). Characterisation of NO production and consumption: New
- insights by an improved laboratory dynamic chamber technique. *Biogeosciences*, 11(19),
- 1285 5463–5492. https://doi.org/10.5194/bg-11-5463-2014





- Benedict, K. B., Prenni, A. J., Carrico, C. M., Sullivan, A. P., Schichtel, B. A., & Collett, J. L.
- 1287 (2017). Enhanced concentrations of reactive nitrogen species in wildfire smoke.
- 1288 Atmospheric Environment, 148, 8–15. https://doi.org/10.1016/j.atmosenv.2016.10.030
- 1289 Burkholder, J. B., Cox, R. A., & Ravishankara, A. R. (2015). Atmospheric Degradation of Ozone
- 1290 Depleting Substances, Their Substitutes, and Related Species. *Chemical Reviews*, 115(10),
- 1291 3704–3759. https://doi.org/10.1021/cr5006759
- 1292 Butterbach-Bahl, K., & Dannenmann, M. (2011). Denitrification and associated soil N2O
- 1293 emissions due to agricultural activities in a changing climate. Current Opinion in
- 1294 Environmental Sustainability, 3(5), 389–395. https://doi.org/10.1016/j.cosust.2011.08.004
- 1295 Crilley, L. R., Kramer, L. J., Ouyang, B., Duan, J., Zhang, W., Tong, S., Ge, M., Tang, K., Qin,
- 1296 M., Xe, P., Shaw, M. D., Lewis, A. C., Mehra, A., Bannan, T. J., Worrall, S. D., Priestley,
- 1297 M., Bacak, A., Coe, H., Allan, J., ... Bloss, W. J. (2019). Intercomparison of nitrous acid
- 1298 (HONO) measurement techniques in a megacity (Beijing). https://doi.org/10.5194/amt-
- 1299 2019-139
- 1300 Crilley, L. R., Lao, M., Salehpoor, L., & VandenBoer, T. C. (2023). Emerging investigator
- series: an instrument to measure and speciate the total reactive nitrogen budget indoors:
- description and field measurements. Environmental Science: Processes and Impacts, 25(3),
- 1303 389–404. https://doi.org/10.1039/d2em00446a
- 1304 Degaspari, I. A. M., Soares, J. R., Montezano, Z. F., Del Grosso, S. J., Vitti, A. C., Rossetto, R.,
- 1305 & Cantarella, H. (2020). Nitrogen sources and application rates affect emissions of N2O
- and NH3 in sugarcane. Nutrient Cycling in Agroecosystems, 116(3), 329–344.
- 1307 https://doi.org/10.1007/s10705-019-10045-w
- 1308 Delaria, E. R., & Cohen, R. C. (2023). Measurements of Atmosphere-Biosphere Exchange of
- Oxidized Nitrogen and Implications for the Chemistry of Atmospheric NOx. Accounts of
- 1310 Chemical Research, 56(13), 1720–1730. https://doi.org/10.1021/acs.accounts.3c00090
- Dennis, R. L., Mathur, R., Pleim, J. E., & Walker, J. T. (2010). Fate of ammonia emissions at the
- local to regional scale as simulated by the Community Multiscale Air Quality model.
- 1313 Atmospheric Pollution Research, 1(4), 207–214. https://doi.org/10.5094/APR.2010.027
- 1314 Ebnesajjad, S. (2017). Introduction to Fluoropolymers. Applied Plastics Engineering Handbook:
- 1315 *Processing, Materials, and Applications: Second Edition*, 55–71.
- 1316 https://doi.org/10.1016/B978-0-323-39040-8.00003-1
- 1317 Edwards, T. M., Puglis, H. J., Kent, D. B., Durán, J. L., Bradshaw, L. M., & Farag, A. M.
- 1318 (2024). Ammonia and aquatic ecosystems A review of global sources, biogeochemical
- cycling, and effects on fish. In Science of the Total Environment (Vol. 907). Elsevier B.V.
- https://doi.org/10.1016/j.scitotenv.2023.167911
- Ellis, R. A., Murphy, J. G., Pattey, E., Van Haarlem, R., O'Brien, J. M., & Herndon, S. C.
- 1322 (2010). Characterizing a Quantum Cascade Tunable Infrared Laser Differential Absorption





1323 Spectrometer (QC-TILDAS) for measurements of atmospheric ammonia. Atmospheric 1324 Measurement Techniques, 3(2), 397–406. https://doi.org/10.5194/amt-3-397-2010 Finlayson-Pitts, B. J., Wingen, L. M., Sumner, A. L., Syomin, D., & Ramazan, K. A. (2003). The 1325 1326 heterogeneous hydrolysis of NO2 in laboratory systems and in outdoor and indoor 1327 atmospheres: An integrated mechanism. Physical Chemistry Chemical Physics, 5(2), 223-1328 242. https://doi.org/10.1039/b208564j 1329 Fowler, D., Coyle, M., Skiba, U., Sutton, M. A., Cape, J. N., Reis, S., Sheppard, L. J., Jenkins, 1330 A., Grizzetti, B., Galloway, J. N., Vitousek, P., Leach, A., Bouwman, A. F., Butterbach-1331 Bahl, K., Dentener, F., Stevenson, D., Amann, M., & Voss, M. (2013). The global nitrogen 1332 cycle in the twenty-first century. Philosophical Transactions of the Royal Society B: 1333 Biological Sciences, 368(1621). https://doi.org/10.1098/rstb.2013.0164 1334 Geddes, J. A., & Murphy, J. G. (2014). Observations of reactive nitrogen oxide fluxes by eddy 1335 covariance above two midlatitude North American mixed hardwood forests. Atmospheric 1336 Chemistry and Physics, 14(6), 2939–2957. https://doi.org/10.5194/acp-14-2939-2014 George, C., Ammann, M., D'Anna, B., Donaldson, D. J., & Nizkorodov, S. A. (2015). 1337 1338 Heterogeneous Photochemistry in the Atmosphere. Chemical Reviews, 115(10), 4218-4258. 1339 https://doi.org/10.1021/cr500648z 1340 Gong, C., Wang, Y., Tian, H., Kou-Giesbrecht, S., Vuichard, N., & Zaehle, S. (2025). 1341 Uncertainties in fertilizer-induced emissions of soil nitrogen oxide and the associated 1342 impacts on ground-level ozone and methane. EGUsphere. 1343 https://doi.org/10.5194/egusphere-2025-1416 1344 González Ortiz, Alberto., Guerreiro, Cristina., & Soares, Joana. (2020). Air quality in Europe: 1345 2020 report. European Environment Agency. https://doi.org/10.2800/786656 1346 Govoni Brondi, M., Bortoletto-Santos, R., Farias, J. G., Farinas, C. S., Ammar, M., Ribeiro, C., 1347 Williams, C., & Baltrusaitis, J. (2024). Mechanochemically Synthesized Nitrogen-Efficient Mg- and Zn-Ammonium Carbonate Fertilizers. ACS Sustainable Chemistry and 1348 1349 Engineering, 12(16), 6182–6193. https://doi.org/10.1021/acssuschemeng.3c07785 1350 Ha, P. T. M., Kanaya, Y., Taketani, F., Andres Hernandez, M. D., Schreiner, B., Pfeilsticker, K., 1351 & Sudo, K. (2023). Implementation of HONO into the chemistry-climate model CHASER (V4.0): Roles in tropospheric chemistry. Geoscientific Model Development, 16(3), 927–960. 1352 1353 https://doi.org/10.5194/gmd-16-927-2023 1354 He, Y., Zhou, X., Hou, J., Gao, H., & Bertman, S. B. (2006). Importance of dew in controlling 1355 the air-surface exchange of HONO in rural forested environments. Geophysical Research 1356 Letters, 33(2). https://doi.org/10.1029/2005GL024348 1357 Huang, G., Zhou, X., Deng, G., Qiao, H., & Civerolo, K. (2002). Measurements of atmospheric 1358 nitrous acid and nitric acid. Atmospheric Environment, 36(13), 2225–2235.

https://doi.org/10.1016/S1352-2310(02)00170-X





- Huber, D. E., Kort, E. A., & Steiner, A. L. (2024). Soil Moisture, Soil NOx and Regional Air
- Quality in the Agricultural Central United States. *Journal of Geophysical Research:*
- 1362 Atmospheres, 129(12). https://doi.org/10.1029/2024JD041015
- 1363 IPCC. (2023). Climate Change 2021- The Physical Science Basis. Cambridge University Press.
- https://doi.org/https://doi.org/10.1017/9781009157896
- 1365 Jang, J.-H., Hong, J., Kim, J. B., Park, S., Hwang, K., Kim, J., Kim, J. Y., Bae, G.-N., Kim, S., &
- 1366 Kim, K. H. (2025). Influence of atmospheric ammonia on secondary inorganic aerosol
- formation in PM2.5 during spring 2024 in the Hongseong area, Republic of Korea.
- 1368 Atmospheric Environment, 121363. https://doi.org/10.1016/j.atmosenv.2025.121363
- Kamboures, M. A., Raff, J. D., Miller, Y., Phillips, L. F., Finlayson-Pitts, B. J., & Gerber, R. B.
- 1370 (2008). Complexes of HNO3 and NO3- with NO2 and N2O4, and their potential role in
- atmospheric HONO formation. *Physical Chemistry Chemical Physics*, 10(39), 6019–6032.
- 1372 https://doi.org/10.1039/b805330h
- 1373 Kamp, J. N., Häni, C., Nyord, T., Feilberg, A., & Sørensen, L. L. (2020). The aerodynamic
- gradient method: Implications of non-simultaneous measurements at alternating heights.
- 1375 Atmosphere, 11(10). https://doi.org/10.3390/atmos11101067
- 1376 Kleffmann, J., Gavriloaiei, T., Hofzumahaus, A., Holland, F., Koppmann, R., Rupp, L.,
- 1377 Schlosser, E., Siese, M., & Wahner, A. (2005). Daytime formation of nitrous acid: A major
- source of OH radicals in a forest. Geophysical Research Letters, 32(5), 1–4.
- 1379 https://doi.org/10.1029/2005GL022524
- 1380 Kolari, P., Bäck, J., Taipale, R., Ruuskanen, T. M., Kajos, M. K., Rinne, J., Kulmala, M., &
- Hari, P. (2012). Evaluation of accuracy in measurements of VOC emissions with dynamic
- chamber system. *Atmospheric Environment*, 62, 344–351.
- 1383 https://doi.org/10.1016/j.atmosenv.2012.08.054
- Kool, D. M., Wrage, N., Zechmeister-Boltenstern, S., Pfeffer, M., Brus, D., Oenema, O., & Van
- Groenigen, J. W. (2010). Nitrifier denitrification can be a source of N2O from soil: A
- revised approach to the dual-isotope labelling method. European Journal of Soil Science,
- 1387 *61*(5), 759–772. https://doi.org/10.1111/j.1365-2389.2010.01270.x
- 1388 Lao, M., Crilley, L. R., Salehpoor, L., Furlani, T. C., Bourgeois, I., Andrew Neuman, J., Rollins,
- 1389 A. W., Veres, P. R., Washenfelder, R. A., Womack, C. C., Young, C. J., & VandenBoer, T.
- 1390 C. (2020). A portable, robust, stable, and tunable calibration source for gas-phase nitrous
- acid (HONO). Atmospheric Measurement Techniques, 13(11), 5873–5890.
- 1392 https://doi.org/10.5194/amt-13-5873-2020
- Laufs, S., Cazaunau, M., Stella, P., Kurtenbach, R., Cellier, P., Mellouki, A., Loubet, B., &
- Kleffmann, J. (2017). Diurnal fluxes of HONO above a crop rotation. *Atmospheric*
- 1395 Chemistry and Physics, 17(11), 6907–6923. https://doi.org/10.5194/acp-17-6907-2017





- Lee, B. H., Lopez-Hilfiker, F. D., Mohr, C., Kurtén, T., Worsnop, D. R., & Thornton, J. A.
- 1397 (2014). An iodide-adduct high-resolution time-of-flight chemical-ionization mass
- 1398 spectrometer: Application to atmospheric inorganic and organic compounds. *Environmental*
- Science and Technology, 48(11), 6309–6317. https://doi.org/10.1021/es500362a
- 1400 Lehnert, N., Musselman, B. W., Seefeldt, L. C., & Gutenberg-university, J. (2021). Grand
- 1401 Challenges in the nitrogen cycle. *Chemical Society Reviews*, 50, 3640–3646.
- 1402 https://doi.org/10.1039/d0cs00923g
- 1403 Li, L., Fan, W., Kang, X., Wang, Y., Cui, X., Xu, C., Griffin, K. L., & Hao, Y. (2016).
- Responses of greenhouse gas fluxes to climate extremes in a semiarid grassland.
- 1405 Atmospheric Environment, 142, 32–42. https://doi.org/10.1016/j.atmosenv.2016.07.039
- 1406 Lipiec, J., Walczak, R., Witkowska-Walczak, B., Nosalewicz, A., Słowińska-Jurkiewicz, A., &
- 1407 Sławiński, C. (2007). The effect of aggregate size on water retention and pore structure of
- two silt loam soils of different genesis. Soil and Tillage Research, 97(2), 239–246.
- 1409 https://doi.org/10.1016/j.still.2007.10.001
- 1410 Liu, L., Zhang, X., Xu, W., Liu, X., Li, Y., Wei, J., Wang, Z., & Lu, X. (2020). Ammonia
- 1411 volatilization as the major nitrogen loss pathway in dryland agro-ecosystems.
- 1412 Environmental Pollution, 265. https://doi.org/10.1016/j.envpol.2020.114862
- 1413 Liu, Zheng, X., Li, Y., Yu, J., Ding, H., Sveen, T. R., & Zhang, Y. (2022). Soil moisture
- determines nitrous oxide emission and uptake. Science of the Total Environment, 822.
- 1415 https://doi.org/10.1016/j.scitotenv.2022.153566
- Ludwig, J., Meixner, F. X., Vogel, B., & Forstner, J. (2001). Soil-air exchange of nitric oxide:
- 1417 An overview of processes, environmental factors, and modeling studies. *Biogeochemistry*,
- 1418 52(3), 225–257. https://doi.org/10.1023/A:1006424330555
- 1419 Luo, X., Zhang, M., Ni, Y., & Shen, G. (2025). Mitigation strategies for NH₃ and N₂O emissions
- in greenhouse agriculture: Insights into fertilizer management and nitrogen emission
- mechanisms. *Environmental Technology and Innovation*, 37.
- 1422 https://doi.org/10.1016/j.eti.2024.103995
- Maggiotto, S. R., Webb, J. A., & Thurtell, G. W. (2000). Nitrous and Nitrogen Oxide Emissions
- from Turfgrass Receiving Different Forms of Nitrogen Fertilizer. *American Society of*
- 1425 Agronomy, Crop Science Society of America, and Soil Science Society of America, 29, 621–
- 1426 630.
- 1427 Mangalassery, S., Sjögersten, S., Sparkes, D. L., Sturrock, C. J., & Mooney, S. J. (2013). The
- 1428 effect of soil aggregate size on pore structure and its consequence on emission of
- greenhouse gases. Soil and Tillage Research, 132, 39–46.
- 1430 https://doi.org/10.1016/j.still.2013.05.003
- Meusel, H., Tamm, A., Kuhn, U., Wu, D., Lena Leifke, A., Fiedler, S., Ruckteschler, N.,
- Yordanova, P., Lang-Yona, N., Pöhlker, M., Lelieveld, J., Hoffmann, T., Pöschl, U., Su, H.,





1433 Weber, B., & Cheng, Y. (2018). Emission of nitrous acid from soil and biological soil crusts 1434 represents an important source of HONO in the remote atmosphere in Cyprus. Atmospheric 1435 Chemistry and Physics, 18(2), 799–813. https://doi.org/10.5194/acp-18-799-2018 Min, K. E., Pusede, S. E., Browne, E. C., LaFranchi, B. W., & Cohen, R. C. (2014). Eddy 1436 1437 covariance fluxes and vertical concentration gradient measurements of NO and NO2 over a 1438 ponderosa pine ecosystem: Observational evidence for within-canopy chemical removal of 1439 NOx. Atmospheric Chemistry and Physics, 14(11), 5495-5512. https://doi.org/10.5194/acp-1440 14-5495-2014 1441 Mochizuki, T., Amagai, T., & Tani, A. (2018). Effects of soil water content and elevated CO2 1442 concentration on the monoterpene emission rate of Cryptomeria japonica. Science of the 1443 Total Environment, 634, 900–908. https://doi.org/10.1016/j.scitotenv.2018.04.025 1444 Moravek, A., Foken, T., & Trebs, I. (2014). Application of a GC-ECD for measurements of 1445 biosphere-atmosphere exchange fluxes of peroxyacetyl nitrate using the relaxed eddy 1446 accumulation and gradient method. Atmospheric Measurement Techniques, 7(7), 2097— 1447 2119. https://doi.org/10.5194/amt-7-2097-2014 1448 Moravek, A., Singh, S., Pattey, E., Pelletier, L., & Murphy, J. G. (2019). Measurements and 1449 quality control of ammonia eddy covariance fluxes: A new strategy for high-frequency 1450 attenuation correction. Atmospheric Measurement Techniques, 12(11), 6059–6078. 1451 https://doi.org/10.5194/amt-12-6059-2019 1452 Mosier, A. R. (2008). Exchange of Gaseous Nitrogen Compounds Between Terrestrial Systems 1453 and the Atmosphere. Nitrogen in the Environment, 443-462. https://doi.org/10.1016/B978-1454 0-12-374347-3.00013-5 1455 Mushinski, R. M., Phillips, R. P., Payne, Z. C., Abney, R. B., Jo, I., Fei, S., Pusede, S. E., White, 1456 J. R., Rusch, D. B., & Raff, J. D. (2019). Microbial mechanisms and ecosystem flux 1457 estimation for aerobic NOy emissions from deciduous forest soils. Proceedings of the 1458 National Academy of Sciences of the United States of America, 116(6), 2138–2145. https://doi.org/10.1073/pnas.1814632116 1459 1460 Neuman, J. A., Trainer, M., Brown, S. S., Min, K. E., Nowak, J. B., Parrish, D. D., Peischl, J., 1461 Pollack, I. B., Roberts, J. M., Ryerson, T. B., & Veres, P. R. (2016). HONO emission and 1462 production determined from airborne measurements over the Southeast U.S. Journal of 1463 Geophysical Research, 121(15), 9237–9250. https://doi.org/10.1002/2016JD025197 1464 Nodeh-Farahani, D., Bentley, J. N., Crilley, L. R., Caputo, C. B., & VandenBoer, T. C. (2021). A 1465 boron dipyrromethene (BODIPY) based probe for selective passive sampling of 1466 atmospheric nitrous acid (HONO) indoors. Analyst, 146(18), 5756-5766. 1467 https://doi.org/10.1039/d1an01089a 1468 Okiti, I., Efakwu, G., Pindus, M., & Kasak, K. (2025). Environmental and biogeochemical drivers of CH4 and N2O flux variability in treatment wetlands. Ecological Engineering, 1469 1470 219. https://doi.org/10.1016/j.ecoleng.2025.107705





- Oswald, R., Behrendt, T., Ermel, M., Wu, D., Su, H., Cheng, Y., Breuninger, C., Moravek, A.,
- Mougin, E., Delon, C., Loubet, B., Pommerening-Röser, A., Sörgel, M., Pöschl, U.,
- Hoffmann, T., Andreae, M. O., Meixner, F. X., & Trebs, I. (2013). HONO emissions from
- soil bacteria as a major source of atmospheric reactive nitrogen. *Science*, 341(6151), 1233–
- 1475 1235. https://doi.org/10.1126/science.1242266
- 1476 Pan, B., Lam, S. K., Mosier, A., Luo, Y., & Chen, D. (2016). Ammonia volatilization from
- 1477 synthetic fertilizers and its mitigation strategies: A global synthesis. *Agriculture*,
- 1478 Ecosystems and Environment, 232, 283–289. https://doi.org/10.1016/j.agee.2016.08.019
- 1479 Pan, B., Xia, L., Lam, S. K., Wang, E., Zhang, Y., Mosier, A., & Chen, D. (2022). A global
- synthesis of soil denitrification: Driving factors and mitigation strategies. *Agriculture*,
- 1481 Ecosystems and Environment, 327(September 2021), 107850.
- 1482 https://doi.org/10.1016/j.agee.2021.107850
- 1483 Pape, L., Ammann, C., Nyfeler-Brunner, A., Spirig, C., Hens, K., & Meixner, F. X. (2009). An
- automated dynamic chamber system for surface exchange measurement of non-reactive and
- reactive trace gases of grassland ecosystems. *Biogeosciences*, 6(3), 405–429.
- 1486 https://doi.org/10.5194/bg-6-405-2009
- 1487 Paulot, F., Jacob, D. J., Pinder, R. W., Bash, J. O., Travis, K., & Henze, D. K. (2014). Ammonia
- emissions in the United States, european union, and China derived by high-resolution
- inversion of ammonium wet deposition data: Interpretation with a new agricultural
- emissions inventory (MASAGE_NH3). Journal of Geophysical Research, 119(7), 4343–
- 1491 4364. https://doi.org/10.1002/2013JD021130
- 1492 Plake, D., Sörgel, M., Stella, P., Held, A., & Trebs, I. (2015). Influence of meteorology and
- anthropogenic pollution on chemical flux divergence of the NO-NO2-O3 triad above and
- within a natural grassland canopy. *Biogeosciences*, 12(4), 945–959.
- 1495 https://doi.org/10.5194/bg-12-945-2015
- 1496 Plake, D., Stella, P., Moravek, A., Mayer, J. C., Ammann, C., Held, A., & Trebs, I. (2015).
- 1497 Comparison of ozone deposition measured with the dynamic chamber and the eddy
- 1498 covariance method. Agricultural and Forest Meteorology, 206, 97–112.
- 1499 https://doi.org/10.1016/j.agrformet.2015.02.014
- 1500 Possanzini, M., Febo, A., & Liberti, A. (1983). New design of a high-performance denuder for
- the sampling of atmospheric pollutants. Atmospheric Environment (1967), 17(12), 2605–
- 1502 2610. https://doi.org/10.1016/0004-6981(83)90089-6
- 1503 Purchase, M. L., Bending, G. D., & Mushinski, R. M. (2023). Spatiotemporal Variations of Soil
- 1504 Reactive Nitrogen Oxide Fluxes across the Anthropogenic Landscape. *Environmental*
- 1505 Science and Technology, 57(43), 16348–16360. https://doi.org/10.1021/acs.est.3c05849
- 1506 Ramazan, K. A., Syomin, D., & Finlayson-Pitts, B. J. (2004). The photochemical production of
- 1507 HONO during the heterogeneous hydrolysis of NO2. *Physical Chemistry Chemical Physics*,
- 1508 6(14), 3836–3843. https://doi.org/10.1039/b402195a





- 1509 Reed, C., Brumby, C. A., Crilley, L. R., Kramer, L. J., Bloss, W. J., Seakins, P. W., Lee, J. D., &
- 1510 Carpenter, L. J. (2016). HONO measurement by differential photolysis. *Atmospheric*
- 1511 Measurement Techniques, 9(6), 2483–2495. https://doi.org/10.5194/amt-9-2483-2016
- 1512 Ren, X., Sanders, J. E., Rajendran, A., Weber, R. J., Goldstein, A. H., Pusede, S. E., Browne, E.
- 1513 C., Min, K. E., & Cohen, R. C. (2011). A relaxed eddy accumulation system for measuring
- vertical fluxes of nitrous acid. Atmospheric Measurement Techniques, 4(10), 2093–2103.
- 1515 https://doi.org/10.5194/amt-4-2093-2011
- 1516 Ren, Y., Stieger, B., Spindler, G., Grosselin, B., Mellouki, A., Tuch, T., Wiedensohler, A., &
- Herrmann, H. (2020). Role of the dew water on the ground surface in HONO distribution: A
- 1518 case measurement in Melpitz. Atmospheric Chemistry and Physics, 20(21), 13069–13089.
- 1519 https://doi.org/10.5194/acp-20-13069-2020
- 1520 Richardson, K., Steffen, W., Lucht, W., Bendtsen, J., Cornell, S. E., Donges, J. F., Drüke, M.,
- 1521 Fetzer, I., Bala, G., Von Bloh, W., Feulner, G., Fiedler, S., Gerten, D., Gleeson, T.,
- Hofmann, M., Huiskamp, W., Kummu, M., Mohan, C., Nogués-Bravo, D., ... Rockström, J.
- 1523 (2023). Earth beyond six of nine planetary boundaries. https://www.science.org
- 1524 Scharko, N. K., Schu, U. M. E., Berke, A. E., Banina, L., Peel, H. R., Donaldson, M. A.,
- 1525 Hemmerich, C., White, R., & Ra, J. D. (2015). Combined Flux Chamber and Genomics
- 1526 Approach Links Nitrous Acid Emissions to Ammonia Oxidizing Bacteria and Archaea in
- 1527 *Urban and Agricultural Soil.* https://doi.org/10.1021/acs.est.5b00838
- 1528 Schindlbacher, A., Zechmeister-Boltenstern, S., & Jandl, R. (2009). Carbon losses due to soil
- 1529 warming: Do autotrophic and heterotrophic soil respiration respond equally? *Global*
- 1530 Change Biology, 15(4), 901–913. https://doi.org/10.1111/j.1365-2486.2008.01757.x
- 1531 Schlesinger, W. H. (2020). Biogeochemistry: An Analysis of Global Change (4th ed.). Academic
- Press. https://doi.org/https://doi.org/10.1016/C2018-0-03255-3

1533 Seinfeld, J. H., & Pandis, S. N. (2006). Atmospheric chemistry and physics: from air pollution to

1534 *climate change.* (2nd edition). John Wiley & Sons.

1535 Shah, S. B., Grabow, G. L., & Westerman, P. W. (2006). Ammonia adsorption in five types of

- 1536 *flexible tubing materials*. https://doi.org/10.13031/2013.22253
- 1537 Song, Y., Xue, C., Zhang, Y., Liu, P., Bao, F., Li, X., & Mu, Y. (2023). Measurement Report:
- Exchange Fluxes of HONO over Agricultural Fields in the North China Plain. July, 1–38.
- https://zenodo.org/record/8115973
- 1540 Sörgel, M., Trebs, I., Wu, D., & Held, A. (2015). A comparison of measured HONO uptake and
- release with calculated source strengths in a heterogeneous forest environment. *Atmospheric*
- 1542 Chemistry and Physics, 15(16), 9237–9251. https://doi.org/10.5194/acp-15-9237-2015
- 1543 Spataro, F., & Ianniello, A. (2014). Sources of atmospheric nitrous acid: State of the science,
- 1544 current research needs, and future prospects. Journal of the Air and Waste Management
- 1545 Association, 64(11), 1232–1250. https://doi.org/10.1080/10962247.2014.952846





- 1546 Stepniewski, W., Stepniewska, Z., & Rozej, A. (2015). Gas Exchange in Soils. Soil
- 1547 *Management: Building a Stable Base for Agriculture*, 117–144.
- https://doi.org/10.2136/2011.soilmanagement.c8
- 1549 Su, H., Cheng, Y., Oswald, R., Behrendt, T., Trebs, I., Meixner, F. X., Andreae, M. O., Cheng,
- 1550 P., Zhang, Y., & Pöschl, U. (2011). Soil nitrite as a source of atmospheric HONO and OH
- radicals. Science, 333(6049), 1616–1618. https://doi.org/10.1126/science.1207687
- 1552 Tang, K., Qin, M., Duan, J., Fang, W., Meng, F., Liang, S., Xie, P., Liu, J., Liu, W., Xue, C., &
- 1553 Mu, Y. (2019). A dual dynamic chamber system based on IBBCEAS for measuring fluxes
- of nitrous acid in agricultural fields in the North China Plain. Atmospheric Environment,
- 1555 196(May 2018), 10–19. https://doi.org/10.1016/j.atmosenv.2018.09.059
- 1556 Tang, K., Qin, M., Fang, W., Duan, J., Meng, F., Ye, K., Zhang, H., Xie, P., Liu, J., Liu, W.,
- Feng, Y., Huang, Y., & Ni, T. (2020). An automated dynamic chamber system for exchange
- 1558 flux measurement of reactive nitrogen oxides (HONO and NOX) in farmland ecosystems of
- the Huaihe River Basin, China. Science of the Total Environment, 745(X), 140867.
- 1560 https://doi.org/10.1016/j.scitotenv.2020.140867
- Tian, H., Pan, N., Thompson, R. L., Canadell, J. G., Suntharalingam, P., Regnier, P., Davidson,
- E. A., Prather, M., Ciais, P., Muntean, M., Pan, S., Winiwarter, W., Zaehle, S., Zhou, F.,
- Jackson, R. B., Bange, H. W., Berthet, S., Bian, Z., Bianchi, D., ... Zhu, Q. (2024). Global
- 1564 nitrous oxide budget (1980-2020). Earth System Science Data, 16(6), 2543–2604.
- 1565 https://doi.org/10.5194/essd-16-2543-2024
- Vaittinen, O., Metsälä, M., Persijn, S., Vainio, M., & Halonen, L. (2014). Adsorption of
- ammonia on treated stainless steel and polymer surfaces. Applied Physics B: Lasers and
- 1568 Optics, 115(2), 185–196. https://doi.org/10.1007/s00340-013-5590-3
- 1569 VandenBoer, T. C., Brown, S. S., Murphy, J. G., Keene, W. C., Young, C. J., Pszenny, A. A. P.
- 1570 P., Kim, S., Warneke, C., De Gouw, J. A., Maben, J. R., Wagner, N. L., Riedel, T. P.,
- Thornton, J. A., Wolfe, D. E., Dubé, W. P., Öztürk, F., Brock, C. A., Grossberg, N., Lefer,
- 1572 B., ... Roberts, J. M. (2013). Understanding the role of the ground surface in HONO
- 1573 vertical structure: High resolution vertical profiles during NACHTT-11. Journal of
- 1574 *Geophysical Research Atmospheres*, 118(17), 10,155-10,171.
- 1575 https://doi.org/10.1002/jgrd.50721
- 1576 VandenBoer, T. C., Young, C. J., Talukdar, R. K., Markovic, M. Z., Brown, S. S., Roberts, J. M.,
- 8 Murphy, J. G. (2015). Nocturnal loss and daytime source of nitrous acid through reactive
- 1578 uptake and displacement. *Nature Geoscience*, 8(1), 55–60.
- 1579 https://doi.org/10.1038/ngeo2298
- 1580 Von Der Heyden, L., Wißdorf, W., Kurtenbach, R., & Kleffmann, J. (2022). A relaxed eddy
- accumulation (REA) LOPAP system for flux measurements of nitrous acid (HONO).
- 1582 Atmospheric Measurement Techniques, 15(6), 1983–2000. https://doi.org/10.5194/amt-15-
- 1583 1983-2022





- 1584 Wang, Fu, X., Wu, D., Wang, M., Lu, K., Mu, Y., Liu, Z., Zhang, Y., & Wang, T. (2021).
- 1585 Agricultural Fertilization Aggravates Air Pollution by Stimulating Soil Nitrous Acid
- Emissions at High Soil Moisture. Environmental Science and Technology, 55(21), 14556—
- 1587 14566. https://doi.org/10.1021/acs.est.1c04134
- 1588 Wang, Y., Fu, X., Wang, T., Ma, J., Gao, H., Wang, X., & Pu, W. (2022). Large Contribution of
- 1589 Nitrous Acid to Soil-Emitted Reactive Oxidized Nitrogen and Its Effect on Air Quality.
- 1590 Environmental Science and Technology. https://doi.org/10.1021/acs.est.2c07793
- 1591 Wolff, V., Trebs, I., Ammann, C., & Meixner, F. X. (2010). Atmospheric Measurement
- 1592 Techniques Aerodynamic gradient measurements of the NH3-HNO3-NH4NO3 triad using a
- wet chemical instrument: an analysis of precision requirements and flux errors. In *Atmos*.
- 1594 Meas. Tech (Vol. 3). www.atmos-meas-tech.net/3/187/2010/
- 1595 Wu, D., Deng, L., Liu, Y., Xi, D., Zou, H., Sha, Z., Pan, Y., Hou, L., & Liu, M. (2020).
- 1596 Comparisons of the effects of different drying methods on soil nitrogen fractions: Insights
- into emissions of reactive nitrogen gases (HONO and NO).
- https://doi.org/10.1080/16742834.2020.1733388
- 1599 Wu, D., Horn, M. A., Behrendt, T., Müller, S., Li, J., Cole, J. A., Xie, B., Ju, X., Li, G., Ermel,
- 1600 M., Oswald, R., Fröhlich-Nowoisky, J., Hoor, P., Hu, C., Liu, M., Andreae, M. O., Pöschl,
- 1601 U., Cheng, Y., Su, H., ... Sörgel, M. (2019). Soil HONO emissions at high moisture content
- are driven by microbial nitrate reduction to nitrite: tackling the HONO puzzle. ISME
- 1603 *Journal*, 13(7), 1688–1699. https://doi.org/10.1038/s41396-019-0379-y
- Wu, D., Zhang, J., Wang, M., An, J., Wang, R., Haider, H., Xu-Ri, Huang, Y., Zhang, Q., Zhou,
- 1605 F., Tian, H., Zhang, X., Deng, L., Pan, Y., Chen, X., Yu, Y., Hu, C., Wang, R., Song, Y., ...
- 1606 Liu, M. (2022). Global and Regional Patterns of Soil Nitrous Acid Emissions and Their
- 1607 Acceleration of Rural Photochemical Reactions. *Journal of Geophysical Research*:
- 1608 Atmospheres, 127(6), 1–16. https://doi.org/10.1029/2021JD036379
- 1609 Yang, J. Y., Drury, C. F., Jiang, R., Worth, D. E., Bittman, S., Grant, B. B., & Smith, W. N.
- 1610 (2024). Reactive nitrogen losses from Canadian agricultural soils over 36 years. *Ecological*
- 1611 *Modelling*, 495. https://doi.org/10.1016/j.ecolmodel.2024.110809
- 1612 Young, C. J., Washenfelder, R. A., Roberts, J. M., Mielke, L. H., Ostho, H. D., Tsai, C.,
- Pikelnaya, O., Stutz, J., Veres, P. R., Cochran, A. K., Vandenboer, T. C., Flynn, J.,
- Grossberg, N., Haman, C. L., Lefer, B., Stark, H., Graus, M., Gouw, J. De, Gilman, J. B., ...
- Brown, S. S. (2012). Vertically Resolved Measurements of Nighttime Radical Reservoirs in
- 1616 Los Angeles and Their Contribution to the Urban Radical Budget.
- Zhang, S., Sarwar, G., Xing, J., Chu, B., Xue, C., Sarav, A., Ding, D., Zheng, H., Mu, Y., Duan,
- 1618 F., Ma, T., & He, H. (2021). Improving the representation of HONO chemistry in CMAQ
- and examining its impact on haze over China. Atmospheric Chemistry and Physics, 21(20),
- 1620 15809–15826. https://doi.org/10.5194/acp-21-15809-2021

https://doi.org/10.5194/egusphere-2025-4662 Preprint. Discussion started: 22 October 2025 © Author(s) 2025. CC BY 4.0 License.





1621	Zhou, S., Young, C. J., VandenBoer, T. C., Kowal, S. F., & Kahan, T. F. (2018). Time-Resolved
1622	Measurements of Nitric Oxide, Nitrogen Dioxide, and Nitrous Acid in an Occupied New
1623	York Home. Environmental Science and Technology, 52(15), 8355–8364.
1624	https://doi.org/10.1021/acs.est.8b01792
1625	Zörner, J., Penning De Vries, M., Beirle, S., Sihler, H., Veres, P. R., Williams, J., & Wagner, T.
1626	(2016). Multi-satellite sensor study on precipitation-induced emission pulses of NOx from
1627	soils in semi-arid ecosystems. Atmospheric Chemistry and Physics, 16(14), 9457–9487.
1628	https://doi.org/10.5194/acp-16-9457-2016
1629	